République Algérienne Démocratique et Populaire

Ministère de l'enseignement Supérieur et de la Recherche scientifique

Université Echahid Hamma Lakhdar – EL OUED

Faculté de La Technologie

Département de Génie électrique

Mémoire de fin d'étude présenté en vue de l'obtention du diplôme de

Master Académique en Electrotechnique

Option : Commande Electrique

THEME

Etude, conception et régulation par PI d'un système photovoltaïque autour de la carte Atmel

Réalisé par :

ALLAG Omar

Encadreur :

Pr. ALLAG ABDELKARIM

Soutenu en Juin 2019

RESUME

Cette thèse est centrée sur l'amélioration des performances et du rendement d'un système photovoltaïque à travers l'utilisation d'un algorithme approprié pour la commande de l'interface de puissance. L'objectif principal est de trouver un algorithme ou une loi de commande efficace et optimale permettant d'extraire le maximum de puissance disponible à partir du générateur photovoltaïque (GPV). Ajoutons à cela, l'étude, la conception et la réalisation d'une unité regroupant un algorithme MPPT et la gestion de l'énergie transmise à la charge (batterie). Les points essentiels traités dans cette étude sont : la modélisation d'un système photovoltaïque, l'étude topologique de l'interface de puissance, l'étude d'un algorithme de poursuite du point de puissance maximale, la simulation d'un convertisseur MPPT, la régulation de la tension photovoltaïque et la conception et la réalisation d'un convertisseur MPPT.

Dans cette investigation, l'algorithme Perturbation et Observation permettant la poursuite du point de puissance maximale est amélioré. L'amélioration principale de l'algorithme permet d'éviter une mauvaise interprétation sur la localisation du MPP lors d'un changement rapide des conditions climatiques. Les résultats de la simulation montrent que l'algorithme MPPT proposé permet d'améliorer le rendement du système photovoltaïque de manière significative.

Dans les systèmes d'alimentation photovoltaïque, le GPV et le convertisseur à commutation présentent des caractéristiques non linéaires et à temps variantes rendant le problème de la commande difficile. La linéarisation des modèles mathématiques permet de se ramener à un problème de commande simple.

L'approche de commande utilisée pour la régulation de la tension photovoltaïque fait appel à un régulateur PID classique. Finalement, la conception et la réalisation d'un convertisseur MPPT à base d'un microcontrôleur visant une gestion énergétique optimale sont décrites.

Mots clés : PV, convertisseur DC-DC, MPPT. P&O, régulateur PID.

ABSTRACT

This thesis focuses on improving performance and efficiency of a PV system with an appropriate algorithm for controlling the power interface. The main objective is to find an effective and optimal algorithm or control law for extracting the maximum available power from the PV generator. Add to this, the study, design and implementation of a unit composed of a MPPT algorithm.

The main points addressed in this study are the modeling of a PV system, the topological study of the power interface, the study of maximum power point tracking (MPPT) algorithms, the simulation of a MPPT converter, the PV voltage regulation and the design and implementation of a MPPT converter.

In this investigation, the Perturb and Observe (P&O) MPPT algorithm is improved. The simulation results show that the proposed MPPT algorithm improves the performances and efficiency of a PV system significantly. In PV power systems, the PV generator and the switch-mode power converter characteristics are nonlinear and time variant making a difficult control problem. The linearization of the mathematical models allows downing to a simple control problem. The approach used is to regulate the PV voltage with a conventional PID controller. Finally, the design and implementation of a MPPT converter based on a microcontroller for an optimal energy management were described.

Key words: PV, converter DC-DC, MPPT, P&O,,PID controller.

ملخص

تركز هذه الرسالة على تحسين أداء وكفاءة النظام الكهروضوئي من خلال استخدام خوارزمية مناسبة للتحكم في واجهة الطاقة. الهدف الرئيسي هو إيجاد خوارزمية أو قانون تحكم فعال ومثالي لاستخراج الطاقة القصوى المتاحة من مولد الطاقة الضوئية .(GPV) أضف إلى ذلك ، الدراسة ، تصميم وتنفيذ وحدة تجميع خوارزمية MPPT وإدارة الطاقة المرسلة إلى الحمل (البطارية). النقاط الرئيسية التي تناولتها هذه الدراسة هي: نمذجة النظام الكهروضوئي ، الدراسة الطوبولوجية لواجهة الطاقة ، دراسة خوارزمية تتبع القدرة القصوى ، محاكاة محول MPPT ، وتنظيم الجهد الكهروضوئي وتصميم وتحقيق محول.MPPT

في هذا التحقيق ، تم تحسين خوارزمية الاضطراب والملاحظة التي تسمح باستمرار أقصى نقطة من القدرة. التحسين الرئيسي للخوارزمية يجعل من الممكن تجنب التفسير الخاطئ لموقع MPP أثناء التغيير السريع في الظروف المناخية. تظهر نتائج المحاكاة أن خوارزمية MPPT المقترحة يمكن أن تحسن بشكل كبير من كفاءة النظام الكهروضوئي.

في أنظمة الطاقة الكهروضوئية ، يتميز GPV ومحول التحويل بخصائص غير خطية ومتباينة للوقت مما يجعل مشكلة التحكم صعبة. يمكن اختزال نماذج النماذج الرياضية إلى مشكلة تحكم بسيطة.

يستخدم نهج التحكم المستخدم في تنظيم الجهد الكهروضوئي منظم PID التقليدي. أخيرًا ، تم وصف تصميم وتنفيذ محول MPPTاستنادًا إلى متحكم دقيق لإدارة الطاقة

الكلمات المفتاحية: منظم PID التقليدي PV ; محول, محول DC-DC ، MPPT، P&O

ACKNOWLEDGEMENT

*I sincerely thank **ALLAH** for helping me study, prepare and successfully complete this thesis.*

*I would like to express my sincere appreciation and gratefulness to my **parents** and **family** for all their support and encouragement during all of my study years and especially during the preparation of this thesis.*

*My very special cordial thanks go to my supervisors **Prof. ALLAG Abdelkrim** for this continuous guidance and valuable discussions resulting in many improvements to the work. I deeply indebted to all teachers in the electrical engineering department for the knowledge and experience I have gained while working under their supervision.*

*I can't forget the help of my fellow colleagues and friends, specially, **Bilal Hammidani , Okba Zeghib** for their continuous guidance and support in my hardest times, also can't forget the generous support of **Oubeidi Nabil** in my lab work.*

Finally, sincere appreciation and thanks to all my friends and colleagues in the Department of Electrical Engineering for their help and being all time on my side.

TABLE OF CONTENTS

Chapter IV: Design and implementation of the P and O around Atmel microcontroller

LIST OF FIGURES

LIST OF SYMBOLS

MPPT	Tracking efficiency
A	Ideal diode quality factor depending on PV technology
C	Capacitor
D	Duty ratio
d	Diode
Dj	Ideal p-n diode
dP	The total power change between two sampling periods
dV	The total voltage change between two sampling periods
Egap	Band-gap energy of the semiconductor used in the cell
fs	dc/dc Converter switching frequency
G	Solar radiation
Gr	Reference solar radiation
11Io	output current of convelmrter
Iom	The maximum output current of the DC/DC converter
Iph	Photocurrent or light generated current
IPV	Output current of the solar cell
IRS	Photovoltaic cell reverse saturation current
IS	Photovoltaic cell dark saturation current
ISC	Short-circuit current of the photovoltaic model
ISC, Ref	Short circuit current at reference condition
KI	Temperature coefficient of the cell’s short circuit current
KSC	PV short circuit current proportional constant
KV	PV open circuit voltage proportional constant
L	Inductance
NP	Number of connected PV cells in parallel
NS	Number of connected PV cells in series
Pmax	Maximum power point
Pout	Output power of the converter
Ppeak	Peak power

List of symbols

Ppv	Output power of the solar cell
RS	Series resistance of the photovoltaic cell
RSh	Shunt resistance of the photovoltaic cell
T	Photovoltaic cell’s operating temperature
TC	Photovoltaic cell’s operating temperature in kelvin
q	The charge of electron
toff	Off period of converter switch
ton	On period of converter switch

GENERAL INTRODUCTION

Brief History of Solar Panels

Solar Panels have become an increasingly popular form of renewable energy. With a simple beginning in the 1800s, photovoltaic (PVs) have continued to be improved and used as a form of energy. In the 1800s, Edmond Becquerel discovered the photovoltaic effect, which led to further research and the eventual invention of the first Photovoltaic Solar Cell in 1883 by Charles Fritts [1]. Since then, improvements have been made to increase efficiency, make solar cells more affordable, and increase their flexibility. The overall project focus was to increase the efficiency of a basic solar panel.

Our Project

The objective of this project was to design a Maximum Power Point Tracker (MPPT) to constantly calculate and maintain the maximum amount of power from a solar panel. By using a DC/DC converter and a microcontroller, I was successfully able to make a system to reach this maximum power.

The solar panel was modeled using a DC voltage source, which then was connected to the DC/DC converter. A buck DC/DC converter was used to step the voltage down. This was required to have the voltage be in the acceptable input range for the microcontroller. Using the microcontroller, a code was created for the Pulse Width Modulation (PWM), which determines the frequency of the PV source. The Perturb and Observe (P&O) method was used to calculate the maximum power the 'PV' source outputs, and the necessary duty cycle for the PWM. That information would then be relayed back to the PV source and adjust it accordingly, to maintain the PV source at the peak power. To test our design, the DC source was adjusted to various voltage inputs, and the maximum power was successfully calculated each time.

This project was made using Matlab Simulink software and implemented using a board, a microcontroller, and a DC voltage source.

Background

As the world continues to develop, the search for renewable energy continues. Not only is renewable energy popular with companies, but with advancements in technology, everyday people are beginning to utilize it. All are also working to dramatically increase the efficiency of appliances, homes, businesses and vehicles [2].

As global temperature rise, wildfires, drought and high electricity demand put stress on the nation's energy infrastructure" [2]. Today, 26% of the world is powered by renewable energy [1]. There are five main types of renewable energy being used. These five are solar, geothermal, bioenergy, wind, and water (hydroelectric). Solar energy is one of the more popular renewable energies, as it accounts for a growing portion of all renewable energy used throughout the world.

Many companies of energy has stated, the development of domestic renewable energy has begun [2]. Solar energy has taken off, as companies such as Solar City have made solar panels more affordable for homeowners. The term "living off the grid" has become more popular and people are using solar power to aid in their sustainable lifestyles. Solar power is so popular among renewable energy because it is essentially free energy. The energy comes from the sun; as long as you live in a location that gets sun light you can have solar power. It is a form of energy that should be accessible for everyone, and that is why solar panels are so important.

How Solar Panels Work?

Solar panels are made of PV cells and other components such as inverters. PV cells are two layers of semiconductor material with opposite charges. When sunlight enters the cell, its energy knocks electrons, which spread in both layers. Due to the opposite charges of the layers, the electrons should move from the N-type layer to P-type layer, however the P-N junction creates an electric field that prevents this from happening and enforces electrons to flow only from the P to N. However, an external circuit connected to the PV cells allows the electrons in the N to travel to P. This electrons flowing through the circuit provide the direct current (DC) electricity. The inverter then converts this DC into alternating current (AC) electricity. The electrical panel then transmits power to lights or other appliances the panels are connected to. Depending on the company that installs the solar panels, the power generated either directly powers appliances/your home or gets fed back to the grid. Most of the time, the power meter or utility meter measures the energy you consume and feeds back to the grid [3].

Solar Panel Efficiency and Availability

As solar panels are becoming increasingly more popular, more research is being done to improve upon them. As of early 2016, the average solar cell is only 15% efficient [4]. As of the fourth quarter of 2016, the efficiency of solar panels is recorded at 22.1% by the First Solar's Cells Break [5]. This means that there is still over 80% of untouched energy that could be used. It is often pointed out that the efficiency of a solar panel varies by brand.

Efficiency is determined by the reflection of the solar panel, and the bandgap energy of the semiconductor within the panel. If the panel has too much reflection, the sunlight isn't absorbed. If the electrons hitting the solar panels have energy higher than the bandgap energy, the photons could pass right through without forming an electron hole pair, which is needed to get energy. The sun puts out a spectrum of radiation and not all of it is light, only some, so it is not possible to harvest 100% of the sun's light with photovoltaics cells. According to physics, the maximum sunlight that can be captured by a photovoltaic cell is approximately 33.7%. The efficiency factor of a solar panel can be because of the silicon that is used to make the solar cell, which is part of a monocrystalline cell. The current commercial monocrystalline cells are only about 24% efficient. So in order to get the best performance of the solar panels, it would be best to make sure that the solar panels get the maximum hours of sunlight during the day, to do that it would need to be clear of shades and the right orientation depending on the time of the day. The maximum power in an ideal situation for a solar panel can be found using the I-V curve. This is the graph of the current vs. the voltage. The peak would be the optimum point of power for the panel [6]. Making all the various adjustments previously discussed would help try and obtain the maximum power, but it would not maintain it. Maintaining the maximum power is the goal of this project.

Even with all of these advancements, solar panels are still sensitive to certain things. Sun intensity can cause the solar panels to become too hot, or can be so weak that the solar panels barely produce any amount of power. Solar panels can also work poorly if they are badly insulated. Bad insulation would cause heat to escape the solar panel and power to be lost. Other methods must be used to monitor the peak efficiency of solar panels to ensure that they are as efficient as they can be.

Maximum Power Point Tracking

As previously stated, other methods need to be employed to monitor and improve efficiency of solar panels. The most popular method is Maximum Power Point Tracking, or MPPT. MPPT is measuring the power of the solar panel at given intervals and making sure it is always at its maximum power. A measurement is taken from the solar panel and the power is calculated. After a specified interval, another measurement is taken. These two measurements are compared, and adjustments are made to the solar panel to ensure that the most recent measurement will lead to the maximum power.

MPPT is not a new technology. Some companies have been designing solar trackers for years. Most solar trackers move with regard to the angle of the sun, and do not constantly calculate power. These trackers are controlled by MPPT controllers. Controllers such as the MPPT Tracer Solar Charge Controller are installed and read a solar panel. Based on the information read, all solar panels are adjusted to follow the sun's path [7].

Though there are some MPPTs already on the market, we has decided to make our own MPPT using a converter and microcontroller. The following work illustrates our thought process during the design of our MPPT, along with results of our working product.

Aim and layout of the thesis

The main objective of this project is to propose and design a board charger with the aim of charging a plug-in vehicle battery. More in detail, different parts of the DC-DC converter have to be designed and simulated. Finally, for the converter a robust and a simple controller have to be implemented and the controllers operation should be verified.

In Chapter 1 a short description about basic concepts and some benefits of this chapter provides an explanation of component characteristics and circuit design and the mathematical modelling of the PV charging a battery(as resistance). It starts with the solar cells, reviewing the physical structure of the semiconductor of the PV cell and the basic concept of how does it convert the sun light into electrical energy. The mathematical model of the solar cell, panel and array are presented and analyzed the effect of the atmospheric conditions on their *I-V* and *P-V* output characteristics. At chapter 2, the main objective is to obtain the maximum power point tracking of the solar panel and many algorithms to execute this process as Perturb and Observe (P&O), and Constant Voltage Method were discussed. Different converters were also presented. In chapter 3, buck converter, filter design, transformer and inductor design criteria were mathematically modelled by using small signal and state variable representation We proposes a design and implementation of a photovoltaic power generation system controller to extract maximum power from the PV panel. Chapter 4 discusses and explains the code used to calculate and maintain the power, and how it was designed and implemented in Matlab/Simulink by using a microcontroller, which adjusts the converter duty cycle by the PWM method, is investigated in this chapter.

Chapter I:

Modelisation and caracterisation of a PV module

I.1 Introduction of PV module:

This chapter provides an explanation of component characteristics and circuit design and the mathematical modelling of the PV charging a battery(as resistance). It starts with the solar cells, reviewing the physical structure of the semiconductor of the PV cell and the basic concept of how does it convert the sun light into electrical energy. The mathematical model of the solar cell, panel and array are presented to show and analyze the effect of the atmospheric conditions on their *I-V* and *P-V* output characteristics.

I.2 The *p-n* junction diode

The symbol of a conventional *p-n* junction diode and its characteristics can be represented as shown in Fig. I.1. The diode is shown below as a blackened triangle with a bar; the triangle suggests an arrow, which gives an indication of the direction in which conventional current flows easily, if a voltage V_D is applied across the diode. Under reverse bias when a voltage is applied to send the current in the reverse direction, only a very small reverse saturation current will flow. In the forward direction, the voltage drop across the diode increases with current, as illustrated in Fig. I.1, and may be less than 1V or above, depending on whether the diode is intended for signal conditioning or power electronic applications [8].

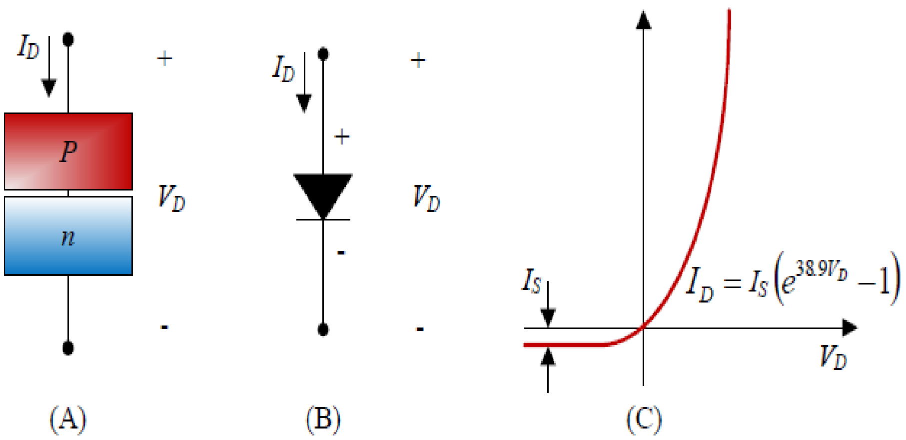

Fig. I.1 a p–n junction diode (A) geometry, (B) symbol and (C) *I-V* characteristic curve.

I.3 Photovoltaic cell

The structure of solar cells is illustrated in Fig.I.2. A semiconductor of *p*-type with a small quantity of added boron atoms forms the substrate. Then atoms of phosphorous are added to the substrate to form a *p-n* junction by applying high-temperature diffusion processing. Near the junction of the two semiconductors, the electrons from the *n*-side diffuse into the p-side leaving behind a layer of ions with positive charge in the *n*-side. In the same manner, the holes in the *p* region diffuse into the n region, which leaves behind a layer of ions with negative charge in the *p*-side. A potential barrier is formed from the rearranged positively and negatively charged ions [9].

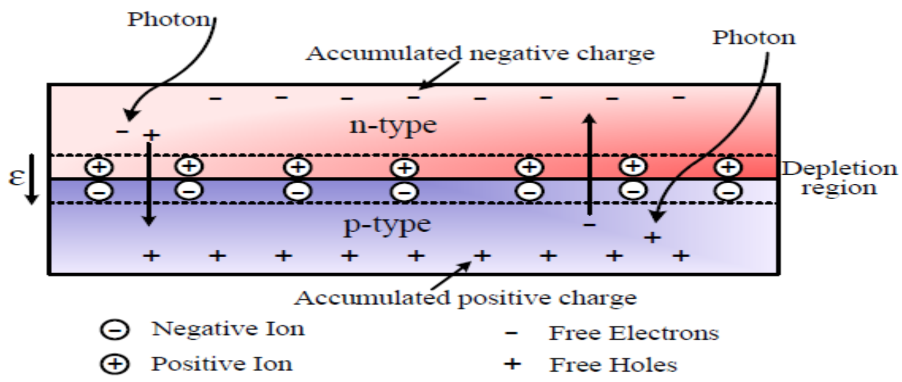

Fig. I.2 Hole-electron pairs created by photons in p-n junction of PV cell

This potential barrier is known as the depletion region and it is free from the mobile charge carriers. The potential barrier also prevents the motion of electrical charges as shown in Fig. I.2. When the structure of p-n is exposed to the sunlight, the electrons in the structure will be excited because of the energy supplied by the photons, and consequently produce hole-electron pairs. These electrical charges are separated by the potential barrier at the p-n junction. At the same time the semiconductors of ***p***-type will extract the holes and electrons will be extracted by the ***n***-type semiconductor. At this moment if an external circuit is connected with n-type and p-type semiconductor of a solar cell as illustrated in Fig. I.3.

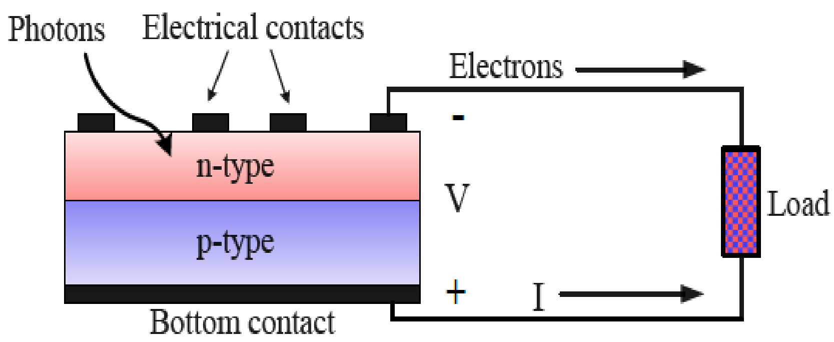

Fig. I.3 Connecting solar with a load and conducting current.

The electrons will move through the external circuit from the n-type semiconductor to p-type in the other side to combine with the holes. This shows how the current in the external circuit is generated. Both sides of the junction are attached with metallic contact in order to collect the electrical current induced by the photons received on one side. The mono-crystalline and poly-crystalline silicon are the most common used material in PV cells. For the most practical applications, the solar cells are connected in series and parallel to multiply the voltage, current and hence power. These cells are put together to form a PV module, and then encapsulated in flat glass to protect them from dust, water etc. [10-12].

I.4 Photovoltaic cell simplified model

There are various mathematical models that have been discussed in the literature to theoretically model photovoltaic cells. All of these models give an approximate behavior of the solar cell. The accuracy of each model is classified according to how many internal phenomena are considered. The basic solar cell is usually represented by a p-n junction diode connected in parallel with current source. This conventional equivalent circuit as illustrated in Fig. I.4 [13,14]. The basic model does not provide a high range of accuracy but it shows the basic behavior of the solar cell.

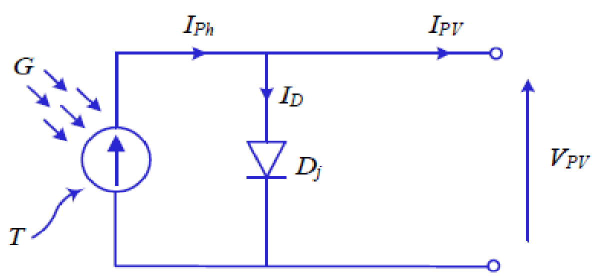

Fig. I.4 Simple model of photovoltaic cell.

The current source represents the photocurrent produced by sunlight and the diode determines the current-voltage characteristic of the cell. The current-voltage characteristic function can be gained by applying Kirchhoff's current law in Fig. I.4 which gives Equation (I.1).

$$I_{PV} = I_{Ph} - I_D \tag{I.1}$$

In the circuit above shown in Fig. I.4, D_j is the ideal p-n diode, I_D the diode internal diffusion current and I_{Ph} the photocurrent, or light generated current, which is proportional to the radiation and surface temperature. The output current and voltage of the solar cell is represented by I_{PV} and V_{PV}, respectively. The diode internal diffusion current is modelled by Equation (I.2).

$$I_D = I_S.\left[exp\left(\frac{q\ .\ V_{PV}}{A\ \cdot\ k\ \cdot\ Tc}\right) - 1\right] \tag{I.2}$$

Where q is the charge of electron, 1.6×10^{-19} C, A is diode ideality factor and it takes the value between 1 and 2, k is Boltzmann's constant, 1.38×10^{-23} J/K, and T_C is the cell's operating temperature in kelvin. The cell dark saturation current, I_S, varies with temperature according to Equation (I.4). The photocurrent, I_{Ph}, is related to the cell's operating temperature and solar intensity as shown in Equation (I.3).

$$I_{Ph} = \left[I_{SC} + K_I \cdot (T_C - T_{Rrf})\right] \cdot \frac{G}{G_r} \tag{I.3}$$

Where I_{SC} is the short-circuit current, is known from the datasheet, K_I is the temperature coefficient of the cell's short circuit (Amperes/ K), T_{Ref} is the cell reference temperature in kelvin, T_{Ref} = 298 K (25 ^oC), G is the solar insolation in W/m^2 and G_r represents the reference solar radiation W/m^2, G_r = 1kW/m^2. Short circuit current is measured under the standard test condition at a reference temperature of 25 ^oC and solar radiation of 1kW/m^2 [13].

$$I_S = I_{RS} \cdot \left(\frac{Tc}{TRef}\right)^{\left(\frac{3}{A}\right)} \cdot exp\left[\frac{q \cdot E_{gap}}{A \cdot\ k}\left(\frac{1}{T_{Ref}} - \frac{1}{T_C}\right)\right] \tag{I.4}$$

In Equation (I.4), I_{RS} is the cell's reverse saturation current in ampere at T_{Ref}, and the solar radiation 1kW/m^2. E_{gap} is the band-gap energy of the semiconductor used in the cell. The cell's reverse saturation current at reference temperature can be obtained by Equation (I.5) [14].

$$I_{RS} = \frac{I_{SC}}{exp\left(\frac{q \cdot V_{OC}}{A \cdot k \cdot T_{Ref}}\right) - 1} \tag{I.5}$$

Where V_{OC} is the open-circuit voltage at reference temperature T_{Ref}.

I.5 Photovoltaic cell general model

The general model is shown in Fig. I.5 is more accurate because it includes the parasitic elements, shunt resistance R_{Sh} and series resistance R_S. Hence the PV cell output current I_{PV}, in Fig.I.5 is given by Equation (I.6).

$$I_{PV} = I_{Ph} - I_S.\left[\left(\frac{q \cdot (V_{PV} + I_{PV} \cdot R_s)}{A \cdot k \cdot T_C}\right) - 1\right] - \left(\frac{V_{PV} + I_{PV} \cdot R_s}{R_{Sh}}\right) \quad \text{(I.6)}$$

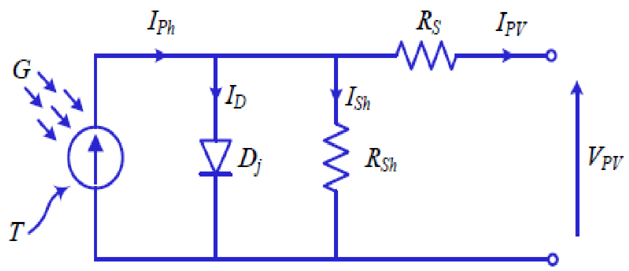

Fig. I.5 More complete general model of photovoltaic cell.

The shunt resistance, R_{Sh}, represents the shunt leakage current to the ground due to pn junction non-idealities and impurities near the junction. The series resistance R_S is due to the bulk resistance of the semiconductor material, the metal contact particularly the front grid and the transverse flow of current in the solar emitter to the front grid. In general the variation of R_{Sh} has no effect on the PV cell short circuit current, I_{SC}, but it reduces the PV cell open circuit voltage as shown in *I-V* characteristic and *P-V* characteristic in Fig. I.6 and Fig. I.7 respectively. Without leakage current to the ground the, R_{Sh}, can be assumed to be infinite. From Fig. I.7, it can be seen that the maximum power point P_{max} in the knee, increases with the increases of R_{Sh} until some extend then the increases of R_{Sh} will have no effect on the P_{max}.

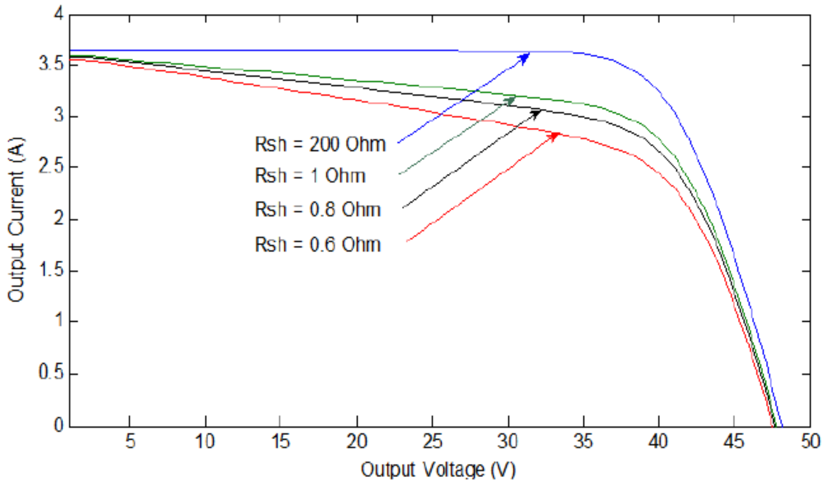

Fig. I.6 Effect of shunt resistance on the *I-V* characteristic

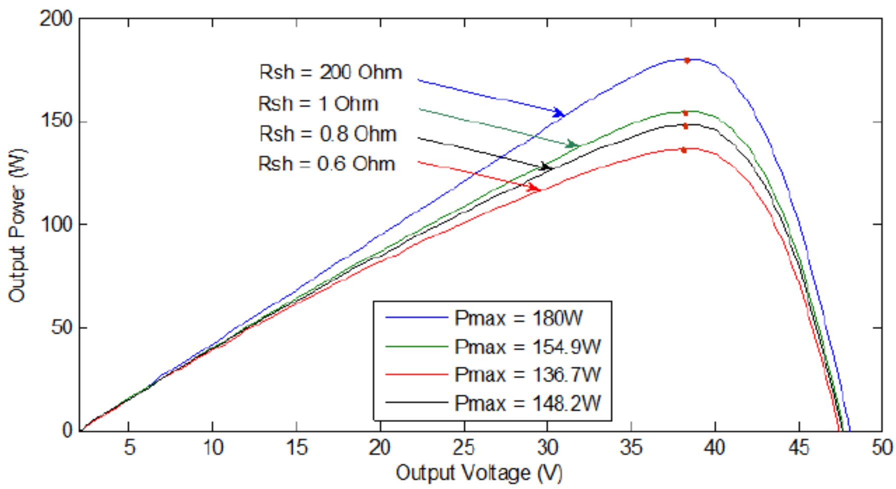

Fig. I.7 Effect of shunt resistance on the *P-V* characteristic

On the other hand, a small variation in R_S leads to a reduction in the short-circuit current but has no effect on the open-circuit voltage as in Fig. I.8, therefore the maximum power changes significantly as depicted in Fig. I.8 and Fig. I.9 [14].

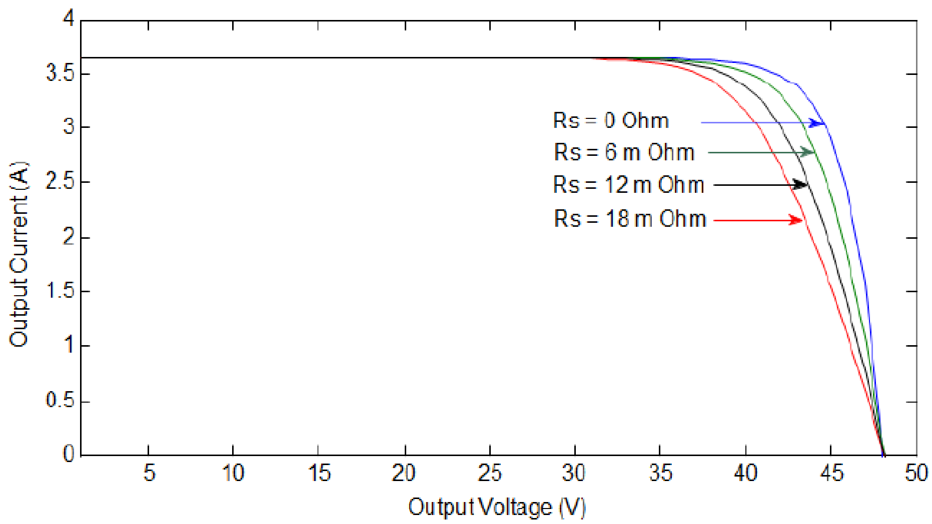

Fig. I.8 Effect of series resistance on the *I-V* characteristic

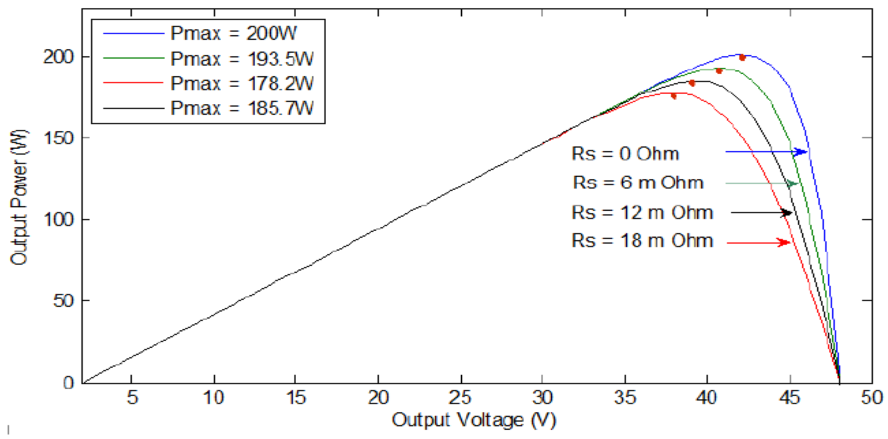

Fig. I.9 Effect of series resistance on the *P-V* characteristic

I.6 Photovoltaic cell appropriate model

As mentioned above, the small variation in R_S has a significant effect on the output power of the PV panel. On the other hand, the PV efficiency is insensitive to the variation in R_{Sh}, which can be assumed to approach infinity without leakage current. Therefore, the R_{Sh} can be neglected to give the appropriate model with suitable complexity. And the effect of R_{Sh} on the *I-V* characteristic and *P-V* characteristic of the PV array is shown in Fig.I.6 and Fig.I.7 respectively [13]. Neglecting the shunt resistance, the model of PV cell becomes an appropriate model with suitable accuracy as shown in Fig. I.10 and Equation (I.6) can be written as:

$$I_{PV} = I_{Ph} - I_S \cdot \left[\left(\frac{q \cdot (V_{PV} + I_{PV} \cdot R_S)}{A \cdot k \cdot T_C}\right) - 1\right] \quad (I.7)$$

The value of R_S is provided in the datasheet by some manufactures. However, if is not provided, the equation of R_S can be derived by differentiating the Equation (I.7) and rearranging in terms of R_S.

$$dI_{PV} = 0 - I_s \cdot q\left(\frac{dV_{PV} + R_S \cdot dI_{PV}}{A \cdot k \cdot T_C}\right) \cdot e^{q\left(\frac{dV_{PV}+R_S \cdot dI_{PV}}{A\,.\,k\,.\,T_C}\right)} \tag{I.8}$$

$$R_S = -\frac{dI_{PV}}{dV_{PV}} - \frac{A\,.\,k\,.\,{}^{T_c}/_{q}}{I_S.\,e^{q\left(\frac{V_{PV}+R_S.I_{PV}}{A\,.\,k\,.\,T_C}\right)}} \tag{I.9}$$

Then by evaluating the Equation (I.9) under the open circuit voltage condition when $V_{PV} = V_{OC}$ and $I_{PV} = 0$.

$$R_S = -\left.\frac{dV_{PV}}{dI_{PV}}\right|_{V_{OC}} - \frac{A\,.\,k\,.\,{}^{T_c}/_{q}}{I_S.\,e^{q\left(\frac{V_{OC}}{A\,.\,k\,.\,T_C}\right)}} \tag{I.10}$$

In Equation (I.10); $\left.\frac{dV_{PV}}{dI_{PV}}\right|_{V_{OC}}$ is the slope of the *I-V* curve at the V_{OC}.

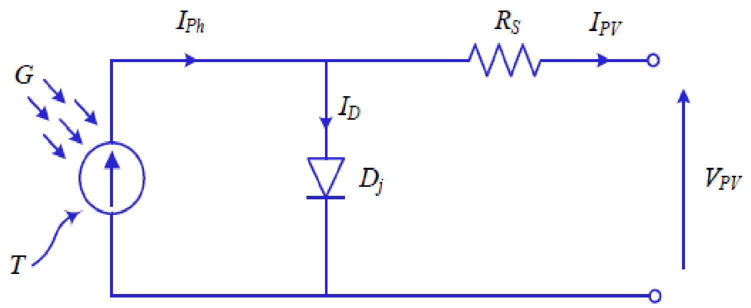

Fig. I.10 Appropriate equivalent circuit model

It is possible for the Equation (I.7) of *I-V* characteristics to be solved. However, the inclusion of a series resistance in the model makes finding a solution complex. Although the answer can be found by using Newton's method [9].

The Newton's method is described as follows:

$$x_{n+1} = x_n - \frac{f(x_n)}{f'(x_n)} \tag{I.11}$$

$f'(x)$ is the derivative of the function, $f(x) = 0$, x_n is present value, and x_{n+1} is a next value.
Rewriting the Equation (I.7) yields the following equation:

$$f(I_{PV}) = I_{Ph} - I_{PV} - I_S \cdot \left[exp\left(\frac{q \cdot (V_{PV} + I_{PV}.\ R_S)}{A \cdot k \cdot T_C}\right) - 1\right] = 0 \qquad (I.12)$$

Substituting Equation (I.12) into (I.11) yields the following equation, and the output current I_{PV} is computed iteratively by using Newton's equation

$$I_{PV(n+1)} = I_{PV(n)} - \frac{I_{Ph} - I_{PV(n)} - I_S \cdot \left[exp\left(\frac{q \cdot \left(V_{PV} + I_{PV(n)} \cdot R_S\right)}{A \cdot k \cdot T_C}\right) - 1\right]}{-1 - I_S .\left(\frac{q \cdot R_S}{A \cdot k \cdot Tc}\right) .\ exp\left(\frac{q.\left(V_{PV} + I_{PV(n)} \cdot R_S\right)}{A \cdot k \cdot T_C}\right)} \qquad (I.13)$$

By using MATLAB/Simulink, the **Characteristics of *I-V*** functions can be computed using Simulink program in Fig I.11

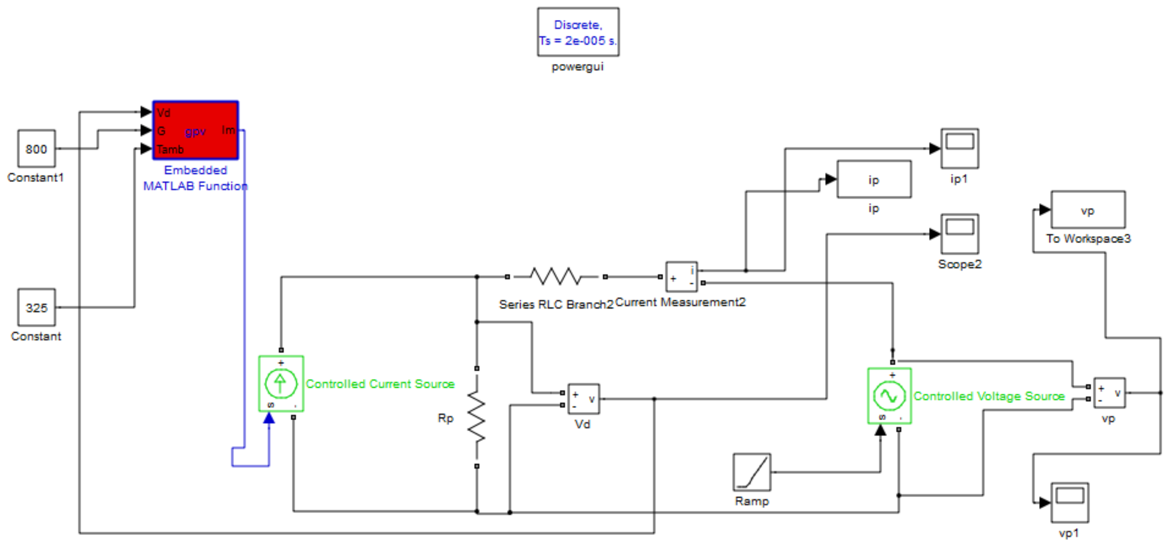

Fig.1.11 Simulink program of the *IPV -VPV* characteristic curve of GPV generator panel solar.

The electrical performance of the solar cell is always described by two factors, the short circuit current I_{SC} and the open circuit voltage V_{OC}. The I_{SC} is the point where the curve intersects with the vertical axis and it is the maximum possible current in the circuit and it is expressed in amps.

This is measured by connecting the positive and negative terminals of the cell together. When the terminals are shorted the output voltage of the circuit is zero.

V_{OC} is the point where the curve intersects with the horizontal axis and represents the maximum possible output voltage from the circuit. This occurs when the PV cells are connected to a very large resistance or in case of no load. Under the condition of open circuit the current is zero.

The power drawn by the photovoltaic module at any point along the curves are shown in Fig. I.6 and Fig. I.8 is expressed in watts. Since the voltage is zero under a short circuit current condition and the current is zero under the open circuit, the output power will be zero at these points.

I.7 Fill factor (*FF*)

The fill factor of photovoltaic generator is defined as the ratio of output power at MPP to the power result from multiplying V_{OC} by I_{SC} as in the Equation (I.15). It determines the shape of the photovoltaic generator characteristic as shown in Fig.I.12. The fill factor plays an important role when comparing the performance of different photovoltaic cells. A high fill factor is equal to a high quality cell which has low internal losses.

$$FF = I_{MPP} \cdot V_{MPP} I_{SC} \cdot V_{OC} = Area\ B\ Area\ A \quad (I.14)$$

After simple multiplication the following equation results

$$ISC \cdot VOC\ FF = IMPP \cdot VMPP = Pmax \quad (I.15)$$

Where I_{MPP} is the current at MPP and V_{MPP} is the voltage at MPP. The fill factor ranges from material to material and it can be seen that it is always < 1. The closer the fill factor is to unity the better the operation of PV cell. The factors which affect (*FF*) are the shunt and series resistances of the photovoltaic generator as shown above in Fig.I.6 to Fig. I.9. A good fill factor is between (0.6-0.8) [7].

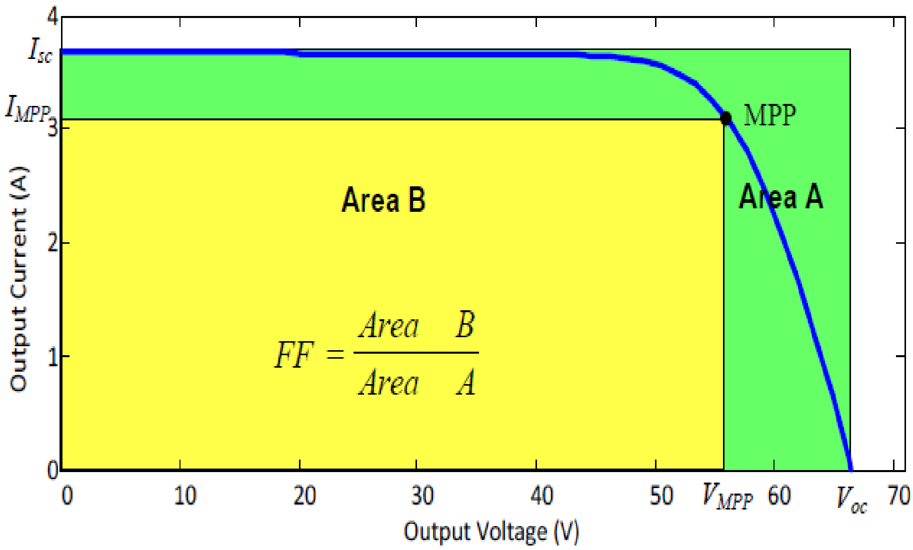

Fig. I.12 Photovoltaic module characteristics showing the fill factor.

I.8 Effect of temperature

The panel temperature is considered one of the important parameters due to its effect on the output power of photovoltaic panel [10, 11].

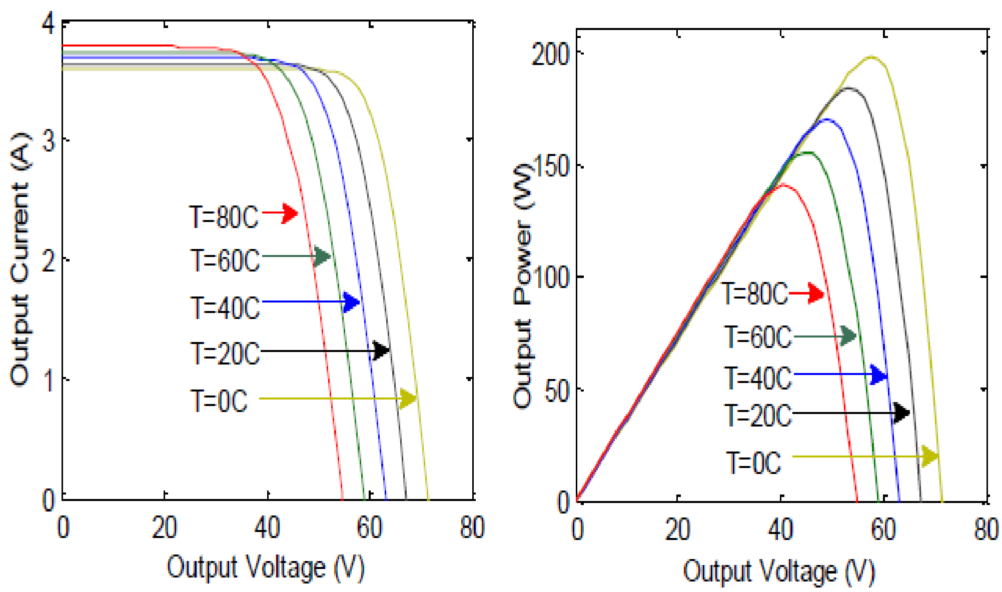

Fig. I.13 Effect of temperature on the *I-V* and *P-V* characteristic at constant irradiance.

The open circuit voltage V_{OC} is highly influenced by the increase in the panel temperature as shown in the Fig. I.13. As the temperature increases with a fixed irradiation level it results in a slight increase in the short circuit current I_{SC}, because the band gap energy decreases and more photons have enough energy to create electron-hole pairs. On the other hand, the increase of temperature have an obvious reduction in the PV panel output power due to the drop in the open circuit voltage *V_{OC}* and the fill factor; therefore the module efficiency is reduced [1].

I.9 Effect of irradiation

At constant temperature the change in irradiation has a clear effect on the PV output maximum power as illustrated in Fig. I.14 [10,11]. It is obvious that as the irradiation level increases the PV output voltage and current increases with it. In general, the increment in the irradiation level leads to a theoretical increment in the maximum power voltage when there is no change in the cell temperature. On the other hand, the short circuit current *I_{SC}* depends totally and linearly on the irradiance level; therefore the maximum power current is changed as shown in Fig. I.14 [11].

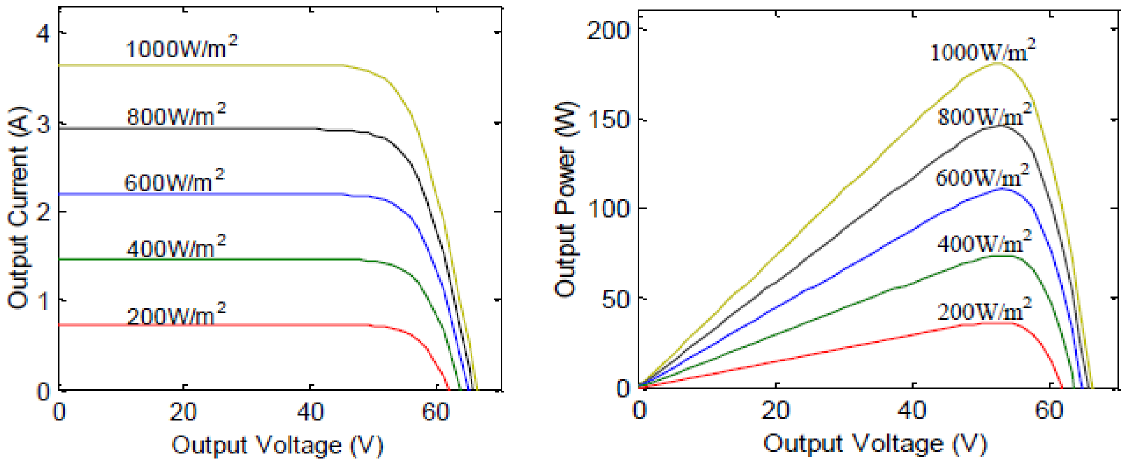

Fig. I.14 Effect of irradiance on the *I-V* and *P-V* characteristic at constant temperature.

I.10 PV module and array module

The typical output power of solar cells in general is very low. It is normally less than 2W at 0.5V. Therefore, the photovoltaic cells are connected in particular configurations so as to form an array which is called a photovoltaic module. In general, the modules consist of group of cells connected in series and parallel to provide the desired output power and voltage as depicted in Fig. I.15. In addition to that, for a photovoltaic system a group of several PV modules are connected in parallel and series in form of PV array to generate the required voltage and current values for the system. When two or more solar panels are wired in series, the same current flows through each panel and the output voltage is the sum of the voltages generated by each panel. Hence, Equation (I.7) can be written as

$$I_{PV} = N_P . I_{Ph} - N_p . I_S . \left[\exp\left(\frac{q}{A \cdot K \cdot T_C} \left(\frac{V_{PV}}{N_S} + I_{PV} \cdot \frac{R_S}{N_P} \right) \right) - 1 \right] \tag{I.16}$$

In contrast, when the solar panels are wired in parallel the output current becomes the sum of the currents from each panel, and the output voltage remains the same.

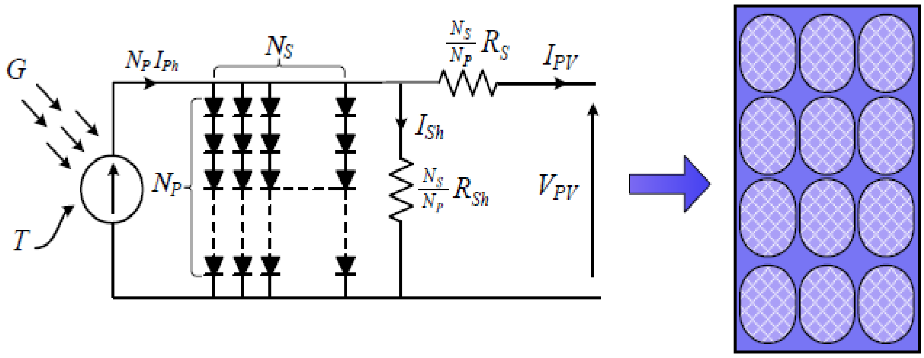

Fig. 1.15 Solar model in parallel and series branches.

I.11 Solar I-V characteristics with resistive load

As can be seen in Fig. I.16 and I.17, the simulation program and the operating characteristic of a solar cell consists of two main regions: the voltage source region and current source region. The voltage source region is located at the right of *I-V* curve and the internal impedance of the solar cell in this region is low. Where the current source region is located on the left of the *I-V* curve and the internal impedance in this region is high. Additionally, it can be observed from the *I-V* curve, that the output current remains almost constant while the terminal voltage changes in the current source region. But in the voltage source region over wide range of output current the terminal voltage has only slight changed.

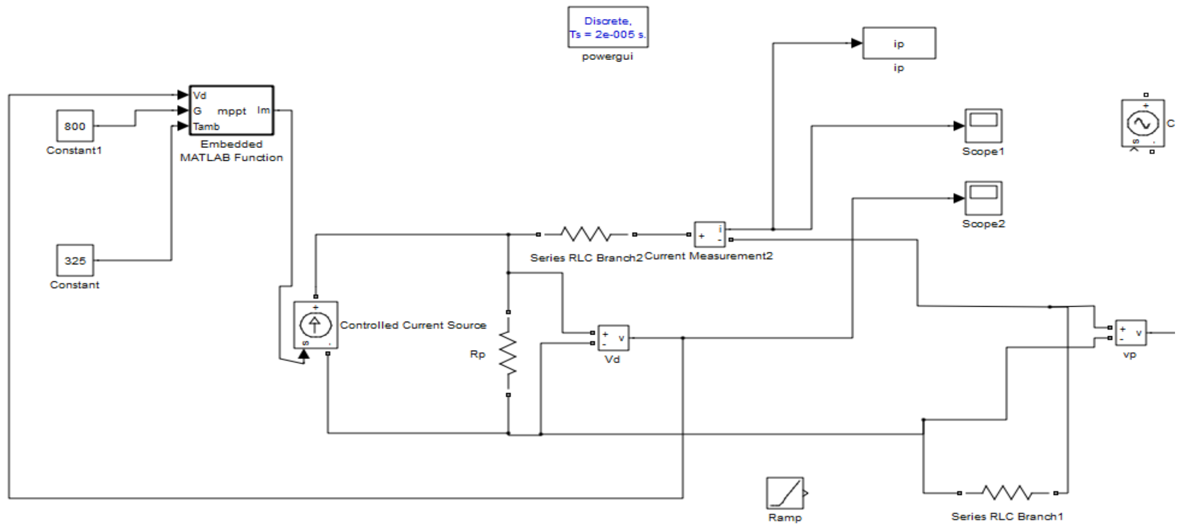

Fig. I.16 Simulink program of PV with resistive load=Rc

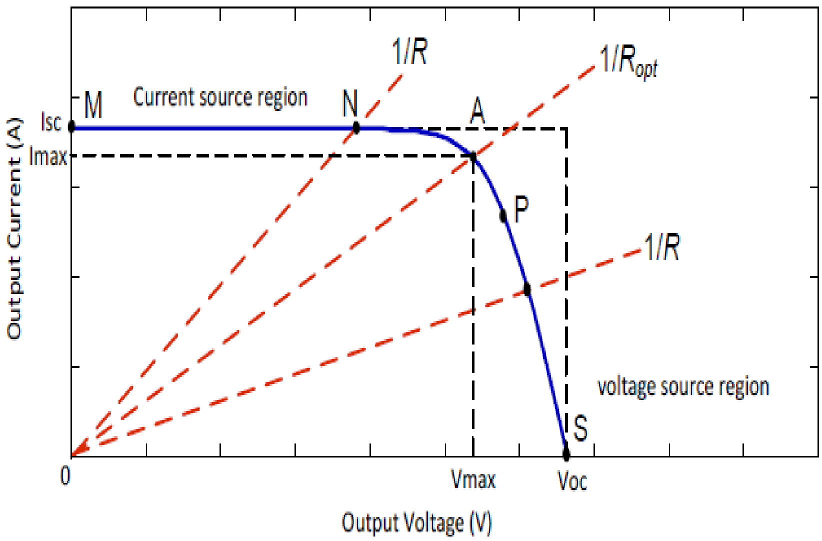

Fig. I.17 Intersection of the I_{PV}-V_{PV} characteristic curve and the load characteristic.

I.12 Interfacing the PV array to the load through DC-DC converter

This section presents how to maximize the power delivered from the PV array to the load at all insolation levels. A buck converter with the output filter, which is essentially a step-down converter, also known as a chopper, inserted between the PV array and the load as shown in Fig. I.18 is a solution to transfer the maximum power.

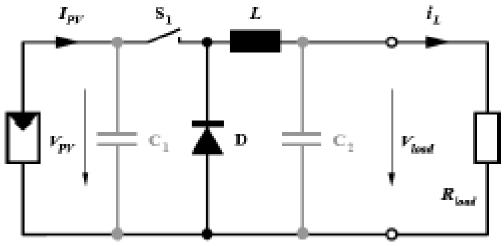

Fig. I.18 PV array supplying R load through step-down converter.

In block diagram shown above, the maximum power can be transferred to the load by the chopper when it is driven with optimal duty ratio *D*. The peak power *Ppeak* delivered to the load under steady-state conditions at any solar insolation levels can be derived.

When a fixed resistive load (*R*) is connected directly to the PV cell's terminals, the operating point is determined by the intersection of the solar cell *I-V* characteristic with the *I-V* characteristic of the load. As shown in the Fig. I.17, the characteristic of the resistive load is a straight line with a slope, $I/V = 1/R$ [12, 13]. Additionally, the power delivered to the load depends only on the resistance value. If the load resistance is small, the cell operates in the current source region MN of the curve, almost near to the short circuit current. Alternatively, if the load resistance is large, the cell operates on the voltage source region PS of the curve, almost near to the open circuit voltage [14].

From Fig. I.16 it is clear that, the operating point may not be at the point (A) which is the maximum power point (MPP) of the PV array. Furthermore, the output characteristics of PV cells are nonlinear, and the optimum operating point constantly varies with changes in the environmental conditions of solar irradiation and cell temperature. The effects of solar irradiation and cell temperature on the *P-V* and *I-V* characteristics are shown in Fig. I.12 and Fig. I.13 respectively.

Since the MPP depends on factors that are not constant and cannot be controlled, i.e. solar irradiation and temperature, a device capable of tracking the MPP and maintain the operation at this point is needed. A maximum power point tracker is a device capable of tracking the MPP, and this device consists of DC-DC power converter its duty cycle adjusted by MPPT controller will be discussed at the next chapter.

I.13 Summary

In this chapter, the model development for the component parts of the proposed PV system are discussed. It begins with the physical structure of PV cells along with the fundamental concept and principles of converting the solar energy to electrical energy. The modeling of equivalent electrical circuit of PV cell presented and discussed. The model is implemented using MATLAB/SIMULIN to study the PV characteristics. Furthermore, the low output power of the single cell is discussed and how to connect number of cells in series and parallel to form a PV panel and array to meet the desired load power. The effect of temperature and solar radiation on the I-V and P-V characteristics of PV cell also discusses this chapter to show the importance of MPPT in the PV system.

Chapter II: Maximum power point tracking techniques and DC-DC converters

II.1 Introduction

The main objective of maximum power point tracking is to read the voltage and current from the solar panel, perform the calculation for power and then display the power at its maximum. There are many algorithms available to execute this process. Some examples include Perturb and Observe (P&O), Incremental Conductance, Parasitic Capacitance and Constant Voltage Method. Of all the available algorithms, P&O is the most widely used algorithm because of its easy implementation. As for the Incremental Conductance method, it is more complex. However, a pro with this method is that it can be more accurate than the P&O method.

For this project, P&O method was chosen to perform the MPPT algorithm. The output voltage and current from the solar panel constantly feeds the input of the DC/DC converter. Since the type of DC/DC converter chosen for this project is the buck converter, it will step the input voltage down based on the duty cycle. The preset duty cycle for the simulation is 70%, so the voltage from the input of the buck converter will be reduced when measure the output of the panel solar.

The output voltage and current of the panel solar sampled and then calculated for power. The calculated power then gets compared to the previous maximum power, if there is one. For the comparison, if the current power is greater than the previous maximum power and the current voltage is also greater than the previous voltage, then the converter's duty cycle increases. Likewise, if the current voltage is less than previous voltage then the duty cycle decreases. As for the case that current power is less than the previous power, and the current voltage is greater than the previous voltage, according to P&O algorithm, the duty cycle of the buck converter should decrease. However, if the current voltage is less than the previous voltage, then increase the duty cycle. The process described above is in one loop of the code. Before starting the next loop, the current power is set to the previous power if it is greater than the previous power. Then a new loop of the same process which is by starting to measure the new voltage and current that is resulted from the newly set duty cycle of the buck converter.

II.2 Maximum power point tracking (MPPT)

It is very important with photovoltaic generation to operate the system at high power efficiency by ensuring that, the system is always working at the peak power point regardless of changes in load and weather conditions. In other words, transfer the maximum power to the load by matching the source impedance with the load one. To confirm that, an MPPT system has been implemented which enables the maximum power to be delivered during the operation of the solar array and which tracks the variations in maximum power caused by the changes in the atmospheric conditions.

The MPPT system is basically an electronic device inserted between the PV array and the load. This device comprises two essential components, as illustrated in Fig.II.1. A DC-DC switching power converter along with an MPPT control algorithm to operate the PV system in such way it can transfer the maximum capable power to the load.

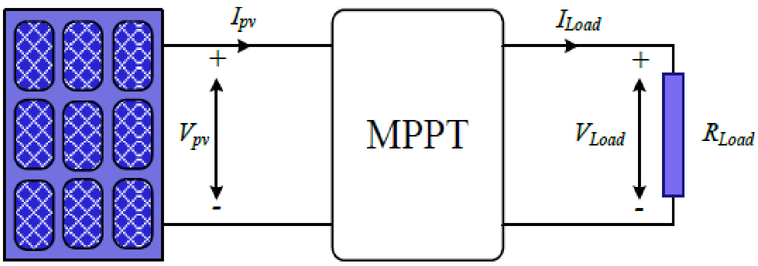

Fig. II.1 Converter acting as a Maximum Power Point Tracker.

As the solar panel outputs power, its maximum generated power changes with the atmospheric conditions (solar radiation and temperature) and the electrical characteristic of the load may also vary. Thus, the PV array internal impedance rarely matches the load impedance. It is crucial to operate the photovoltaic generation system at the MPP or near to it to ensure the optimal use of the available solar energy. The main objective of the MPPT is to match these two parameters by adjusting the duty ratio of the power converter. As the location of the MPP on the *I-V* curve varies in an unpredictable manner it cannot be defined beforehand due to changes of radiation and PV panel temperature. Accordingly, the use of MPPT algorithm or calculating model is required to locate this point [5].

There are several methods to track the MPP of the photovoltaic system that have been carefully studied, developed and published over the last decades. The authors in [5] have presented many MPPT control algorithms, some of which are addressed in the following sections. There are variations between these techniques in terms of, simplicity, sensor requirements, cost, range of efficiency, convergence speed and hardware implementation. Some MPPT algorithms outperform the others under the same operating conditions. A review and analysis of several

MPPT techniques have been carried out in [2] to quantify the performance of each control algorithm compared to the others.

II.3 Performance specifications of MPPT control algorithm

As noted earlier, the dynamic response, steady-state error and tracking efficiency should be considered for a successful design when evaluating the performance of a new or modified MPPT control algorithms [3].

II.3.1 Dynamic response

The response of a MPPT control algorithm needs be fast to track the MPP during the rapid changes in the atmospheric conditions (solar irradiation and temperature). The higher the tracking speed of the MPPT algorithm, the lower the loss in solar energy in the system.

II.3.2 Steady-state error

The MPPT control algorithm should stop tracking, once the MPP is located and should force the system to maintain operation at this optimal operating point as long as possible. However, this is impossible to achieve practically in an actual MPPT system because of the active perturbation process in MPPT algorithms with fixed tracking step-size and the continuous variation in solar insolation and temperature. This phenomenon has a negative impact on the PV system efficiency.

II.3.3 Tracking efficiency

Defining the tracking efficiency is a very important step, to quantify how successfully an MPPT control algorithm tracks the MPP and to what extent it contributes to increase the overall performance of the PV system compared to other methods. According to [4,5] the tracking efficiency is defined as the ratio between the actual power of the PV array and the theoretical power during the same time period. The atmospheric conditions (irradiation and temperature) are changeable and vary over a wide range. Hence, each MPPT algorithm must be evaluated over a range of different operating conditions when comparing MPPT algorithm performance. A well-designed MPPT control system should provide good performance in different atmospheric conditions.

II.4 MPPT algorithms classification

Several MPPT algorithms have been proposed for PV power systems in recent years, to locate the MPP and increase the system efficiency. The MPPT algorithms may be divided into two types, which are indirect control or “quasi tracking techniques” and direct control or “true tracking techniques” [5, 6]. In the indirect control techniques, the MPP is calculated either by measuring the voltage and current of the PV array, the solar insolation, or by the use of mathematical functions obtained from empirical data. Therefore, these techniques are incapable of tracking the MPP with varying irradiation and temperature. The indirect control techniques are look-up table technique, constant voltage technique, fractional open-circuit voltage and fractional short-circuit current. However, the true tracking techniques have the ability to find the optimum operating point even under changing atmospheric conditions, because they do not rely on previous knowledge of or calculated data from the PV array *V-I* characteristics. The true tracking techniques are the perturbation and observation (P&O) technique, incremental conductance (INC) technique and others techniques. In the tracking process one or two variables are used for calculating the MPP. The fractional open-circuit voltage and fractional short-circuit current use only one variable, either the PV array output voltage or current respectively, though the P&O need both variables to determine the MPPT [5, 6] Fig II.2.

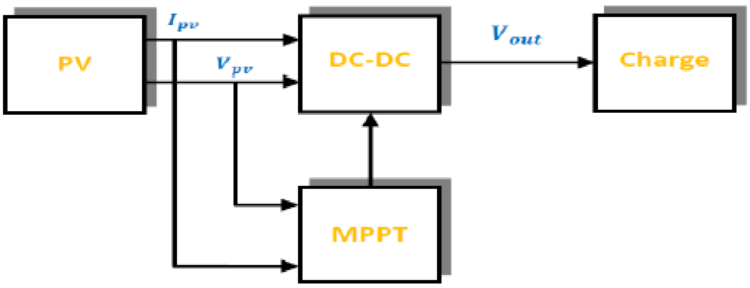

Fig. II.2 Schematic block diagram of the load-matching method.

II.4.1 Constant voltage method (CV)

If the PV system is implemented without a load (battery) to tie the bus voltage to an approximately constant level, a simple control scheme of the constant voltage method can be applied as presented in [6, 7]. In this method the feedback of the PV voltage is compared with a fixed reference voltage and the resultant signal adjusts the duty ratio of the DC-DC converter to keep the operating point of the PV array at the MPP or close to it, as illustrated in Fig. II.3. The reference voltage is set to be equal to the V_{MPP} of the characteristic PV array or to another calculated best fixed voltage.

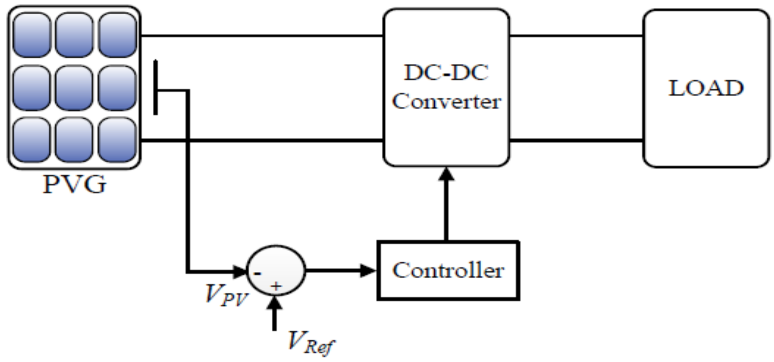

Fig. II.3 Voltage feedback MPPT method with constant voltage reference.

This method is simple, economical and only one feedback-loop control is required. However this technique has the drawback that it does not correct for environmental variation such as change in irradiation and temperature [5].

II.4.2 Perturb and observe (P&O) algorithm

The perturb and observe algorithm is considered to be the most commonly used MPPT algorithm among the other techniques because of its simple structure and ease of implementation. It is based on the concept that on the power-voltage curve, the change in the PV array output power is equal to zero ($\Delta P_{PV} = 0$) on the top of the curve as illustrated in Fig. 2.4 [8]. The P&O operates by periodically perturbing (incrementing or decrementing) the PV array terminal voltage or current and comparing the corresponding output power of PV array $P(n+1)$ with that at the previous perturbation $P(n)$. If the perturbation in terminal voltage leads to increase in the PV power ($\Delta P_{PV} > 0$) the perturbation should be kept in the same direction, otherwise the perturbation is moved to the opposite direction. The perturbation cycle is repeated until reaching the maximum power at ($\Delta P_{PV} = 0$). The control flow chart of P&O is shown in Fig. II.5. There are two different ways to implement the P&O algorithm. In the conventional way a reference voltage is used as a perturbation parameter; therefore a PI controller is needed to adjust the duty ratio. The second way is that, the duty ratio is directly perturbed and the power is measured every PWM cycle. The advantages of this technique are simplicity, ease of implementation and it does not require a previous knowledge of the PV array.

However, the P&O will not stop perturbing when the MPP is reached and will oscillate around it resulting in some unnecessary power loss.

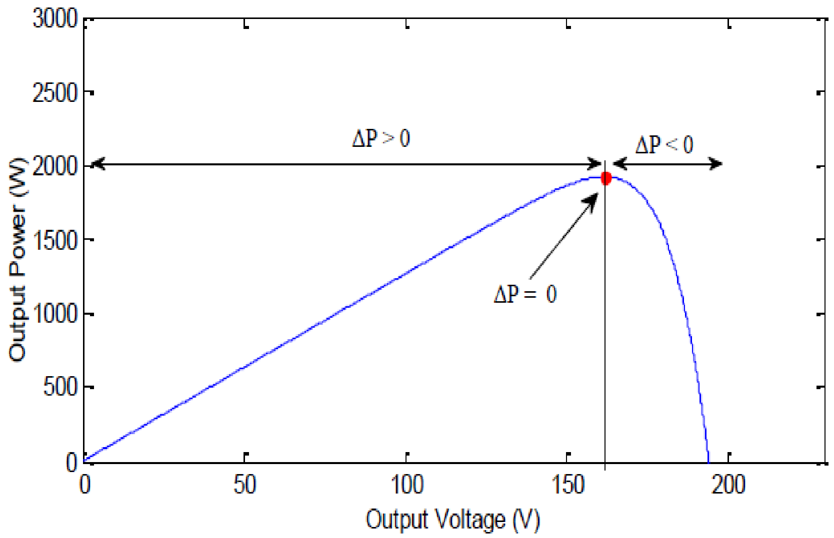

Fig. II.4 Sign of the *dP/dV* at different positions on the power characteristic.

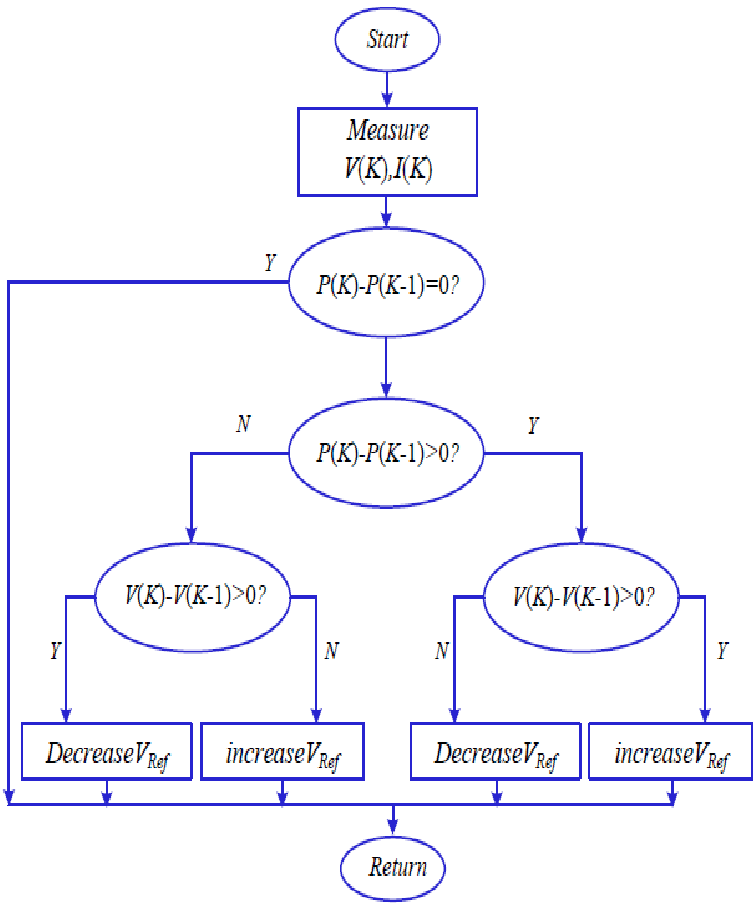

Fig. II.5 Flowchart of the P&O algorithm

II.5 DC-DC converters

The switch mode DC-DC converter is considered the main part of a MPPT system. These are widely used to convert unregulated DC inputs into a controlled DC output at a desired voltage and current levels in DC power supplies and DC motor drives. The same converter is used for a MPPT to provide load matching for the maximum power transfer by regulating the input voltage at the PV array MPP by controlling the duty ratio (*D*).

If the photovoltaic panel is directly connected to a load, its operating point will be defined by the intersection of the load and photovoltaic generation curves as shown in Fig. I.15. Therefore, there is a unique point where the both curves intersect each other, exactly at a MPP. The generation curve nonlinearly changes with the change of the radiation (*G*) and temperature (*T*), while the load curve has a different characteristic according to the type of load is connected to the photovoltaic module. Hence, DC-DC converters are used to interface the photovoltaic module with the load, in order to ensure the photovoltaic module is always operating at the maximum power point. This is done by controlling the converter duty ratio (*D*) with maximum power point tracking algorithms (MPPT).

II.5.1 Topologies

There are several types of DC-DC converters. They are generally categorized into two types: isolated and non-isolated converters. In the isolated topologies a small high frequency electrical isolation transformer is used to provide the DC isolation between the input and output of the DC converter; and step up or down of the output voltage is achieved by changing the transformer turns ratio. These types of converter are used in switch mode power supply [99]. The flyback, half bridge and full bridge are the most commonly used topologies for majority of the applications [5]. Also these types of topology are used in PV grid-tied system when electrical isolation is needed for safety reasons, and to eliminate the possibility of coupling DC to AC grid.

Non-isolated converters do not have an isolation transformer. They are very often used in DC motor drives [7]. Non-isolated converters are classified into three types: step up (boost), step down (buck), and step up & step down (buck-boost).

II.5.2 Buck converter

In this type of DC-DC converter, the average output voltage V_o produced is always lower than the DC input voltage. The buck converter is used for voltage step-down in PV applications, such as for charging batteries and in water pumping systems. The basic circuit of the step-down converter as illustrated bellow in Fig. II.6 [7]. The diode (*d*) is used to enhance the output filtering effect and prevent the switch from absorbing or dissipating the inductive energy because this would lead to overheating the switch. In addition to that, there is an inductor and capacitor at the output of the converter which forms a low-pass filter to attenuate the output voltage fluctuation.

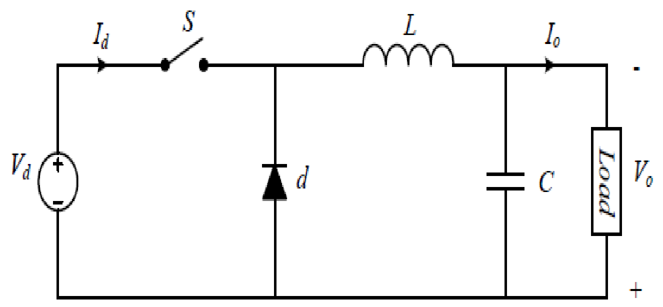

Fig. II.6 Step-down Buck converter.

Fig. II.9 illustrate the wave forms of the inductor current (i_L) and voltage (v_L) of the step-down converter operating in a continuous conduction mode.

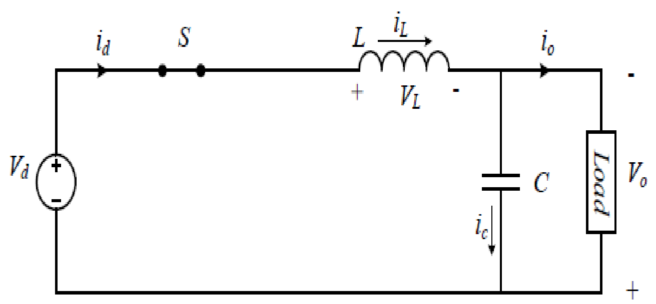

Fig. II.7 Step-down Buck converter switch closed.

At the time duration when the switch *S* is on as shown in Fig. II.7, the diode *d* becomes reverse biased and the input voltage V_d appears across the inductor leading to linear increase in the inductor current i_L. In addition, the capacitor *C* is charged in the same cycle [8].

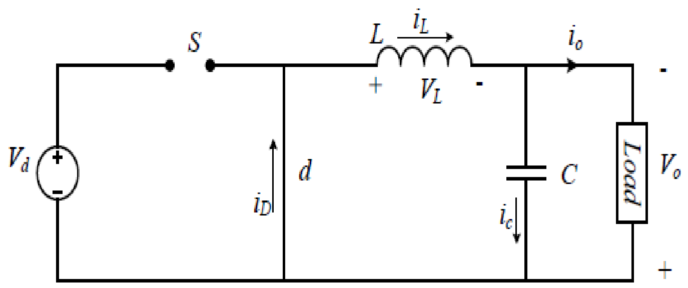

Fig. II.8 Step-down Buck converter switch open.

When the switch *S* is turned off as shown in Fig. II.8, the diode *d* becomes forward biased and the voltage across the inductor is reversed $v_L = -V_o$. Therefore, current in the inductor freewheel through the diode and starts decreasing linearly. In this cycle the capacitor is charged by the inductor energy.

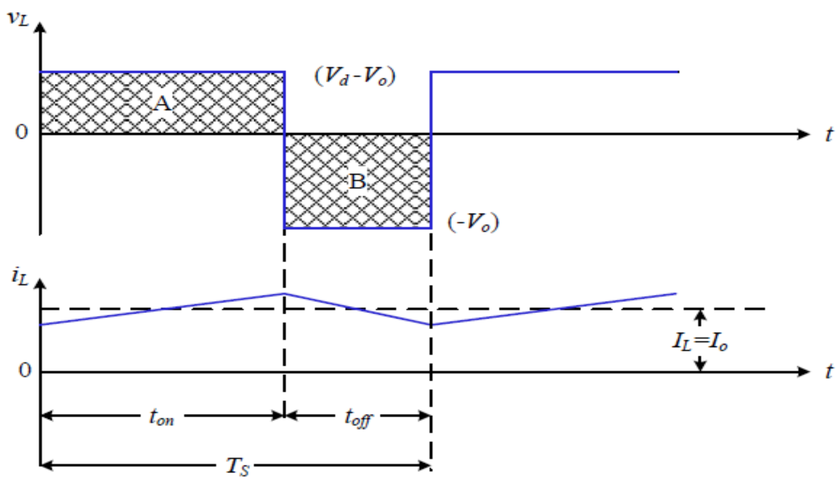

Fig. II.9 Step-down converter wave form of the inductor current and voltage in continuous current mode.

The waveform must repeat from one time period to the next during steady-state operation. The relation between the input and output voltage, input and output current and the duty ratio *D* can be defined by Equation (II.1) and (II.2) [9].

$$\frac{V_o}{V_d} = \frac{t_{on}}{T_s} - D \tag{II.1}$$

$$\frac{I_o}{I_d} = \frac{1}{D} \tag{II.2}$$

$$L = \frac{V_S(1-D)}{2\Delta I_S f_S} \tag{II.3}$$

$$C = \frac{I_o D}{8\Delta V_o f_S} \tag{II.4}$$

In Equations (II.1) and (II.2) T_S is the switching period, or time period of square pulse that controls the electronics switch S, t_{on} is the on time of controlling square wave, I_o is the converter output current, I_d is the converter input current.

II.5.3 Boost converter

Example applications of boost converter operation are the regenerative braking circuit of DC motors and in regulated DC power supplies. In this type of converter the output voltage is always greater than the input voltage. Therefore the step up converter can be applied to MPPT systems where the output voltage needs to be greater than the input voltage. Such as in a grid-connected system where the boost converter maintains a high output voltage even if the PV array voltage falls to low values. The circuit topology of the step-up converter as illustrated in Fig. II.10 [8].

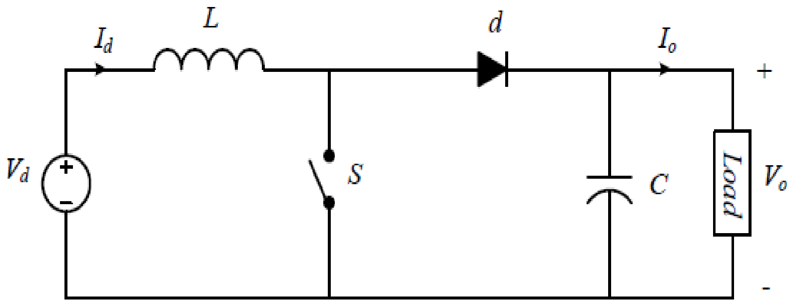

Fig. II.10 Step-up boost converter.

When the switch S is on the diode d is reverse based. Consequently, the current in the inductor L rises linearly due to the input voltage source, and in this case the output stage is isolated and the capacitor C is partially discharged supplying the current load. When the switch is off during the second interval the diode is conducting, and during this time the output stage receives energy from both the inductor and the input source. The wave form of the inductor current during continuous conduction mode is shown below in Fig. II.11 where the inductor current flows continuously, i.e. $I_L(t) > 0$ [8,9].

When the converter is operating at steady-state condition, the duty ratio, D, can be expressed by Equation (II.5) [9].

$$D = 1 - \frac{V_d}{V_o} \tag{II.5}$$

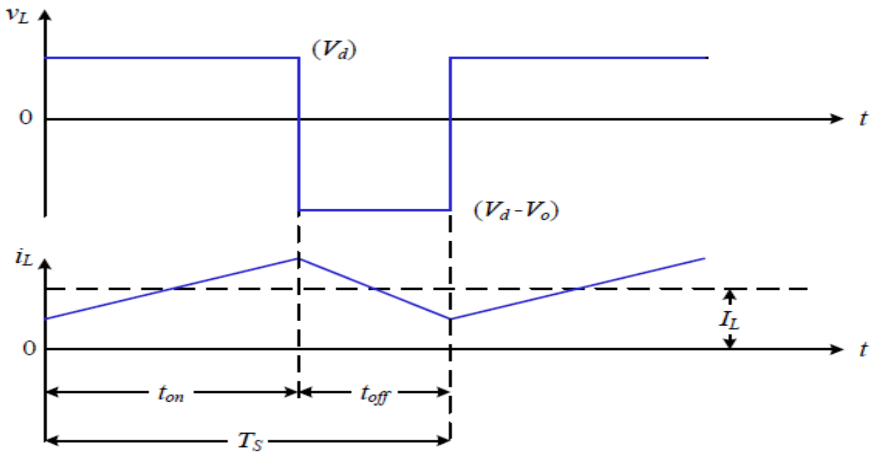

Fig. II.11 Step-up converter wave form of the inductor current and voltage in continuous current mode.

Where D denotes the duty ratio, V_d and V_o denotes the input and the output voltages of the converter, respectively. From the above equation it can be seen that, the increase in the duty ratio D will increase the value of the output voltage, V_o. In addition the change in the duty ratio results in change in the input and the output current of the converter. The filter inductor and capacitor to operate the converter in the continuous conduction mode can be calculated by the following equations:

$$L = \frac{V_d D}{2\Delta I_L f_s} \tag{II.6}$$

$$C = \frac{I_o D}{\Delta V_o f_s} \tag{II.7}$$

II.5.4 Buck-Boost converter

A Buck-Boost converter is cascade connection of two basic converters, the buck converter and boost converter. The Buck-Boost converter provides an output voltage can be higher or lower than the input voltage. Also this type of converter produces a negative polarity output with respect to the common terminal of the input voltage [7]. The main application of Buck-boost converter is in regulated DC power supplies. Fig. II.12 shows the circuit topology of Buck-Boost converter [8, 9].

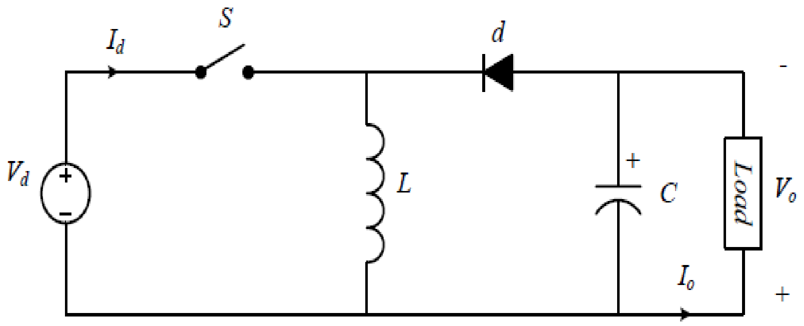

Fig. II.12 Buck-boost converter.

In the equivalent circuit shown in Fig. II.12 when the switch *S* is turned on during the first time interval t_{on} of the switching period T_S, the diode *d* is reverse based and input provides energy to the inductor causing the inductor current i_L to increase as illustrated in Fig. II.13. When the switch is off during the second time interval t_{off}, the diode is forward biased so the energy stored in the inductor is transferred to the load. In this case the inductor current i_L is forced to flow backwards through the load and results in a negative polarity in the converter output voltage.

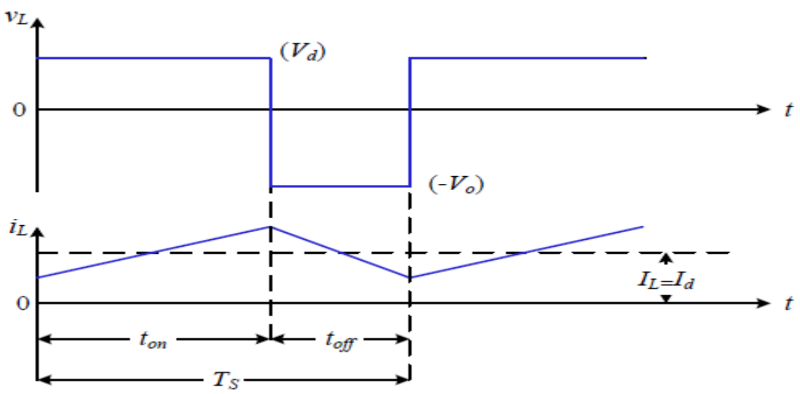

Fig. II.13 Step-down converter waveform of the inductor current and voltage in continuous current mode

During the steady-state condition the relation between the output voltage V_o and the duty ratio of the converter can be defined by the following equation.

$$\frac{V_o}{V_d} = \frac{D}{1 - D} \quad \text{(II.8)}$$

From the above equation the output voltage could be higher or lower than the input voltage according to the value of the duty ratio. For the duty ratio condition $D > 0.5$, the output is higher than the input as in a boost converter. If $D < 0.5$ the output is lower than the input as in a buck converter.

$$L = \frac{(1 - D)^2 R}{2 f_s} \quad \text{(II.9)}$$

$$C = \frac{D}{R f_s (\Delta V_o / V_o)} \quad \text{(II.10)}$$

II.6 Mathematical models of DC-DC converters connected to PV generator

II.6.1 Buck case:

Based on schematic of the buck converter given in Fig. II.15 ,we can found

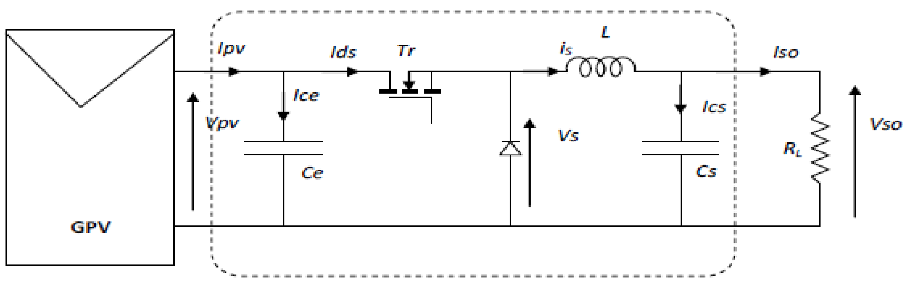

Fig. II.14 PV system connected to buck converter

a)Adaptation conditions :

$$R_i = R_{pv} = \frac{V_{pv}}{I_{pv}} \quad \text{(II.11)}$$

From the previous equations the input resistance of the converter becomes

$$R_i = R_L \frac{1}{\delta^2} \tag{II.12}$$

From where

$\lim_{\infty \to 0} R_i = +\infty$ and $\lim_{\infty \to 1} R_i = R_L$

The input resistance of the Buck therefore varies in the meantime $[R_L \quad \infty[$

b) State Model :

For : $t \in [0 \,.\, \delta T]$ T_I closes D blocks and the switch closed mode ON

$$\begin{cases} \frac{di_L}{dt} = \frac{1}{L}\left(V_{pv} - V_{so}\right) \\ \frac{dV_{so}}{dt} = \frac{1}{C}\left(i_L - \frac{V_{so}}{R}\right) \end{cases} \quad 0 < t < \delta T.ON \tag{II.13}$$

And when switch is open mode OFF

$$\begin{cases} \frac{di_L}{dt} = \frac{1}{L}\left(-V_{so}\right) \\ \frac{dV_{so}}{dt} = \frac{1}{C}\left(i_L - \frac{V_{so}}{R}\right) \end{cases} \delta T < t < T.OFF \tag{II.14}$$

II.6.2 Boost case:

Based on schematic of the buck converter given in Fig.II.16 ,we can found

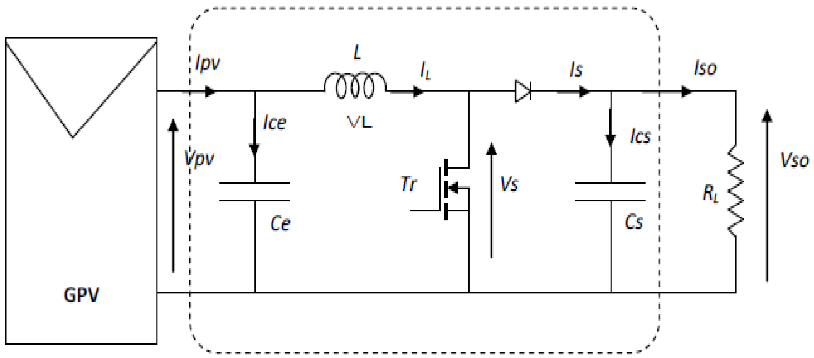

Fig. II.15 PV system connected to boost converter

a) Adaptation conditions

$$R_i = R_{pv} = \frac{V_{pv}}{I_{pv}} \quad \text{(II.15)}$$

From the equation we deduce

$$R_i = R_L.(1-\delta)^2 \quad \text{(II.16)}$$

From where $\lim_{\infty \to 0} R_i = R_L$ *and* $\lim_{\infty \to 1} R_i = 0$

The input resistance therefore varies in the meantime $[0 \quad R_L]$

b) State Model :

$$\begin{cases} Ice = Ce.\frac{dVpv}{dt} = I_{pv} - I_L \\ Ics = Cs.\frac{dVso}{dt} = -I_{so} \qquad 0 < t < \delta T \\ V_L = L.\frac{dI_L}{dt} = V_{pv} \end{cases} \quad \text{(II.17)}$$

$$\begin{cases} Ice = Ce.\frac{dVpv}{dt} = I_{pv} - I_L \\ Ics = Cs.\frac{dVso}{dt} = I_L - I_{so} \qquad \delta T < t < (1-\delta)T \\ V_L = L.\frac{dI_L}{dt} = V_{pv} - V_{so} \end{cases} \quad \text{(II.18)}$$

II.6.3 Buck-Boost case:

Based on schematic of the buck-boost converter given in Fig. II.17 ,we can found

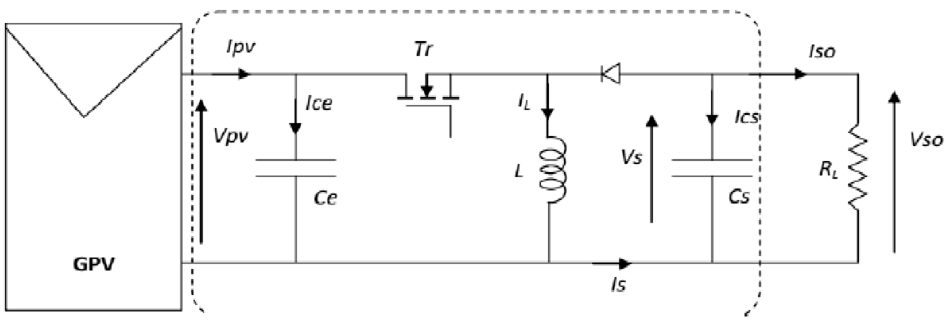

Fig. II.16 PV system connected to Buck-Boost converter

a) Adaptation conditions :

In continuous regime we have:

$$R_i = R_{pv} = \frac{V_{pv}}{I_{pv}} \qquad \text{(II.19)}$$

$$R_i = \left(\frac{1-\delta}{\beta}\right)^2 . R_L \qquad \text{(II.20)}$$

From where $\lim_{\delta \to 0} R_i = +\infty$ *and* $\lim_{\delta \to 1} R_i = 0$

The input resistance of the Converter Buck-Boost can therefore take any value between[0 ∞[. The point of maximum power can therefore be reached regardless of the value of the load.

b) State Model :

The two differential equation systems governing the operation of the converter Buck-Boost

$$\begin{cases} Ice = Ce.\dfrac{dVpv}{dt} = I_{pv} - I_L \\ Ics = Cs.\dfrac{dVso}{dt} = -I_{so} \\ V_L = L.\dfrac{dI_L}{dt} = V_{pv} \end{cases} \qquad 0 < t < \delta.T \qquad \text{(II.21)}$$

$$\begin{cases} Ice = Ce.\dfrac{dVpv}{dt} = I_{pv} \\ Ics = Cs.\dfrac{dVso}{dt} = -I_L - I_{so} \\ V_L = L.\dfrac{dI_L}{dt} = V_{so} \end{cases} \qquad \delta T < t < T \qquad \text{(II.22)}$$

II.7 Summary

This chapter reviews and discuses MPPT techniques for solar PV systems that are discussed in the literature along with their advantages and disadvantages. Besides that, this chapter presents a comparison between these techniques in terms of steady-state oscillation, tracking speed and efficiency. The comparison suggest that, based on MPPT efficiency, the P&O techniques have the potential to perform better than the other MPPT techniques. However, because of the higher implementation cost of other techniques, its use would not be justified by the relatively small improvement in the performance. This makes the P&O technique more attractive than other technique in this work.

In addition, many types of DC-DC converters have been studied to see which converter is suitable for the MPPT stage of the PV system. In the literature [103-107], a comparative analysis from different viewpoints has been made between some commonly used topologies to track the maximum power of the PV array. Some of them are known as single inductor types, such as the Buck, Boost and Buck-Boost converters. In many reference showed that, the Buck-Boost converter has the advantage over individual Buck and Boost converters of following the MPP at all times, under any conditions of solar global radiation, cell temperature and connected load.

Chapter III: Modelling, Controller design and Simulations of the GPV-DC-DC converter

III.1 Introduction:

The energy produced by the photovoltaic systems is very intermittent and depends enormously on the weather conditions. This is why it is important to find a way to store this energy. We proposes a design and implementation of a photovoltaic power generation system controller. As to extract maximum power from the PV panel, the proposed system controls both the buck converter and the battery charger using a microcontroller. The proposed solution is based on the Arduino microcontroller.

III.2 GPV-Power DC-DC converter Model:

For simplicity some assumptions have been made:

(1) Transformer leakage inductance and resistance, on-state resistance of switch and inductance and ESR of capacitance, all are neglected due to very small values does not have any obvious effect at practical gain.
(2) The battery load is assumed to be purely resistive.

In order to design a robust controller for the GPV- converter Fig.III.1, the first step is to find the plant transfer function. There are several methods for doing this [11], but as we are only interested in the small signal method which will be briefly explained in the following section will be used.
In [4], a step by step procedure of obtaining the GPV- power stage and output filter transfer function of a DC-DC converter, will be explained.

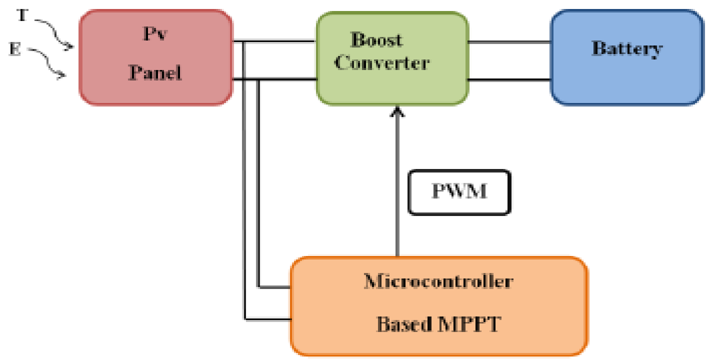

Fig. III.1.Block diagram of the battery voltage regulator with MPPT.

The proposed standalone photovoltaic (PV) system consists of three main blocks: PV panel, power converter and MPPT controller. The following sections will describe the modeling of the PV panel and power converter.

III.2 .1. Load Model (battery):

The following circuit Fig.III.2 represents the model of the battery, which is given by the following equation

$$V_{bot} = E - R_0 I_{bat} + V_{C_b}$$

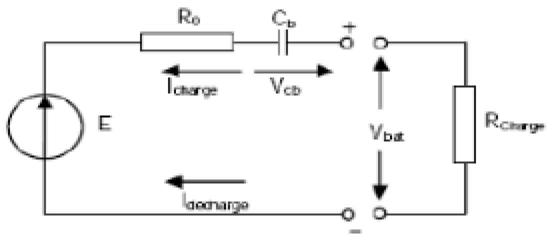

Fig. III.2 Electrical model of the battery

For our application, we consider that the model will be represented by a resistance Load R0.

III.2.2 GPV Panel Model:

The GPV model represents the solar cell in its simplest form as a PN junction followed by a series resistance as shown in Fig. III.3 [12]. The PV system equivalent circuit was described in chapter I by nonlinear equations, such that the dynamic resistance r_{pv} is given by:

$$i_{pv} = n_p I_{ph} - n_p I_{rs}(e^{\frac{k_{pv} v_{pv}}{n_s}} - 1) \qquad \text{(III.1)}$$

Such that

$$K_{pv} = \frac{q}{pKT} \;, I_{rs} = T_{rr}\left(\frac{T}{T_r}\right)^3 e^{\frac{qEgp(\frac{1}{T_r}-\frac{1}{T})}{pk}} \;,\; I_{ph} = (I_{sc} + K_i(T - T_r))\frac{\lambda}{100}$$

and

$$R_S = r_{pv} = -\left.\frac{dV_{PV}}{dI_{PV}}\right|_{V_{OC}} - \frac{A\cdot k\cdot T_C/q}{I_S\cdot e^{q\left(\frac{V_{OC}}{A\cdot k\cdot T_C}\right)}}$$

III.2.3 Power DC-DC converter circuit Model

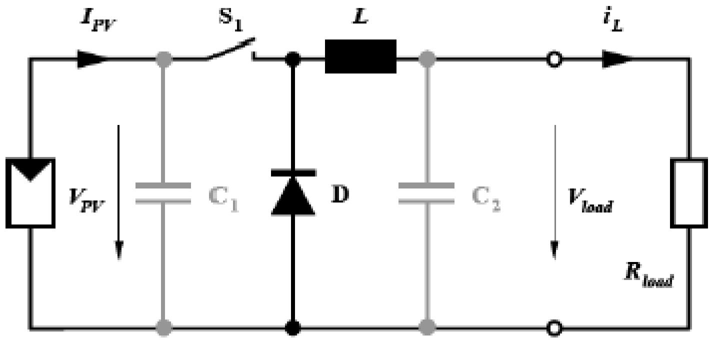

Fig. III.3. Power DC-DC converter electric circuit

First, we can obtain for each state (switch **on** and switch **off** S) the corresponding circuit state and state space matrix equations. The circuit state for switch **on** and **off** can be simplified to Fig. III.4 a) and b):

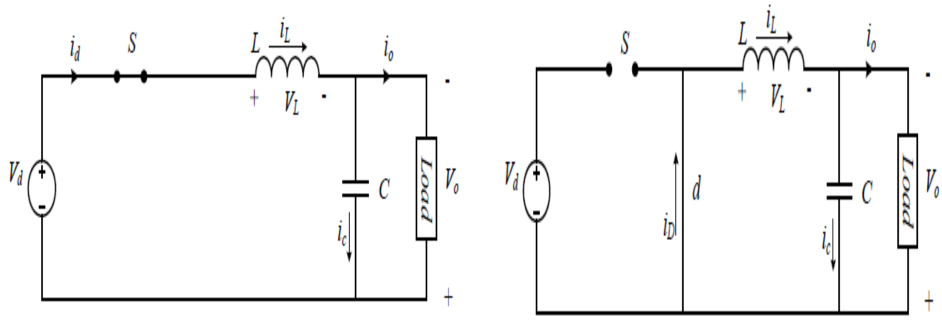

a) b)

Fig. III.4 Circuit state for switch on a) and off b).

In continuous mode conduction, Fig III.5 represents waveform responses of the mains variables:

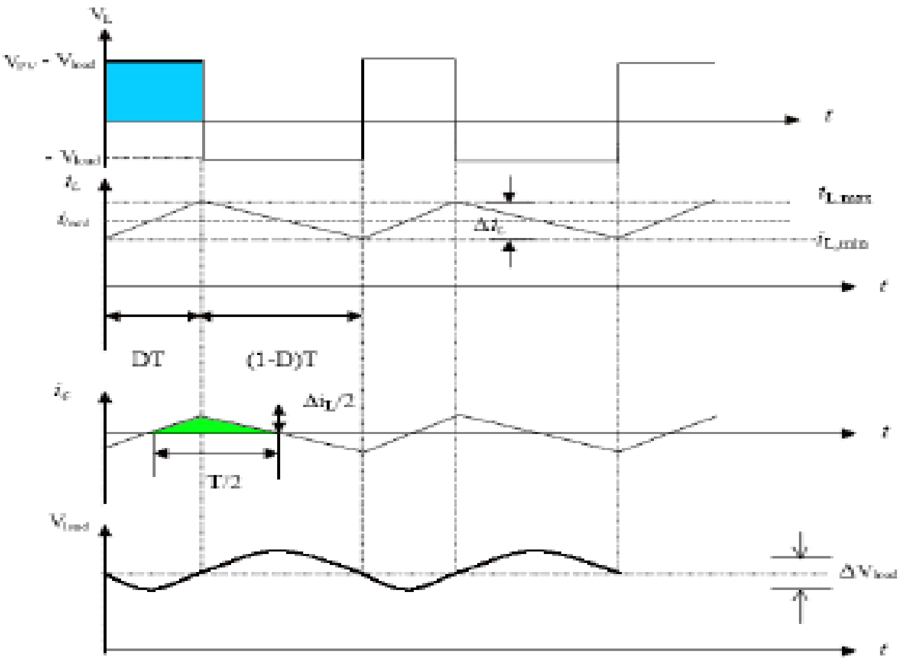

Fig. III.5 Waveform responses of the mains variables

III.3 Output filter design for buck converter

Referring to wave forms response of the converter of Fig. III.5**,** the presence of L and C2 in the output of DC-DC converter create a low pass filter with cut off frequency:

$$f_C = \frac{1}{2\pi\sqrt{L.C_2}} \tag{III.2}$$

We also know that:

$$\Delta_{i_L.on} + \Delta_{i_L.off} = 0 \Longrightarrow V_{load} = D.V_{PV} \tag{III.3}$$

And the Power equivalent:

$$V_{PV}.I_{PV} = V_{load}.I_{load} = D.V_{PV}.I_{load} \tag{III.4}$$

Then

$$I_{load} = \frac{I_{PV}}{D}$$

The output voltage ripple is calculated based on the basic equation of capacitor C2:

$$\Delta V_{C_2} = \frac{\Delta Q}{C_2} = \frac{1}{C_2} \cdot \frac{1}{2} \cdot \frac{\Delta i_L}{2} \cdot \frac{T}{2} = \frac{\Delta i_L}{8 \cdot C_2 \cdot fs}$$

$$= \frac{V_{load}}{8 \cdot L \cdot C_2 \cdot fs^2} \cdot (1 - D) = \frac{V_{PV}}{8 \cdot L \cdot C_2 \cdot fs^2} \cdot (1 - D) \cdot D \tag{III.5}$$

$$\frac{\Delta V_{C_2}}{V_{C_2}} = \frac{(1-D)}{8 \cdot L \cdot C_2 \cdot fs^2} \quad \text{(III.6)}$$

L- calculation:

We assume that all the output ripple currents (harmonics) will pass through capacitor and only DC (average value of) current will be delivered to the load. This assumption enables us using basic equation of inductors.

By the help of Fig.III.5, we can write for the output ripple currents:

:

$$\frac{\Delta i_L}{I_{L.moy}} = \frac{(1-D)}{L \cdot fs} \cdot R_{load} \quad \text{(III.7)}$$

If we consider D=0.5

$$L \geq \frac{(1-D)}{4 \cdot \Delta i_{L.max} \cdot fs} \quad \text{(III.8)}$$

And by defining the desired voltage ripple and having all the parameters and L from previous calculations, C2 can be found

In order to filter the switching frequency ripple, we need to have fc set less than 0.2fs.

C2- Calculation:

For maximum duty cycle D=0.5

$$\Delta V_{C_{2.max}} = \frac{V_{PV}}{32 \cdot L \cdot C_2 \cdot fs^2}$$

Consequently, the capacity value is given by:

$$C_2 \geq \frac{V_{PV}}{32 \cdot L \cdot \Delta V_{C_{2.max}} \cdot fs^2} \quad \text{(III.9)}$$

Finally ;we obtain

$$C_2 \geq \frac{\Delta i_{L.max}}{8 \cdot \Delta V_{C_{2.max}} \cdot fs} \quad \text{(III.10)}$$

If $f_C = \frac{1}{2\pi\sqrt{L.C_2}}$

Then $$\frac{\Delta V_{C_2}}{V_{C_2}} = \frac{\pi^2}{2} \cdot (1-D) \cdot \left(\frac{f_C}{fs}\right)^2 \quad \text{(III.11)}$$

III.4 Transfer function of GPV-DC-DC-Load

III.4.1 State model and transfer function of DC-DC Converter

The developed standalone PV system uses a buck converter as a power-processing unit. The buck converter circuit consists of a MOSFET switch and a freewheeling diode, in addition to a rectifier circuit based on a capacitor and an inductor as shown in Fig.III.6 The circuit is controlled through a PWM signal generated by the MPPT controller. The state-space averaging technique is used to generate the low-frequency small-signal ac equations of the PWM DC-DC converter [13]. The buck converter is assumed to operate in a continuous conduction mode while switching between two states depending on the switch position (ON/OFF). In the first state, (0≤t≤ton), the switch will be ON, and in the second state, (ton≤t≤T), the switch will be OFF.

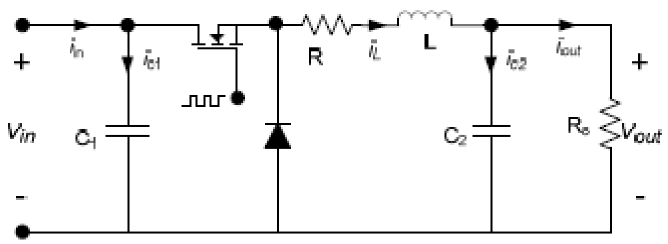

Fig. III.6 Real buck converter circuit.

Taking the inductor current i_L , output voltage v_{out} , and input voltage v_{in} as state variables, the converter equations can be derived and written in state-space form for each switch state using $U = i_{pv}$ as the system input, $V_{in} = v_{pv}$ as the system output, and $x = [i_L \; v_{out} \; v_{in}]$ the state vector.

$$d(t) = \frac{t_{on}(t)}{T} \tag{III.12}$$

The duty cycle is considered to be a time varying quantity. It is assumed that the natural frequencies of the converter network are much smaller than the switching frequency. The converter waveforms are expressed as quiescent (nominal) values plus small ac variations as follows [13]:

$$\begin{cases} x(t) = X + \hat{x}(t) \\ u(t) = U + \hat{u}(t) \\ y(t) = Y + \hat{y}(t) \\ d(t) = D + \hat{d}(t) \end{cases} \tag{III.13}$$

The small-signal ac model is then obtained as:

$$\begin{cases} \text{the state} \quad \frac{d\dot{\hat{x}}(t)}{dt} = A\hat{x}(t) + Bu(t) + Md(t) \\ \text{And the output} \quad y(t) = C\hat{x}(t) + F\hat{u}(t) + H\hat{d}(t) \end{cases} \tag{III.14}$$

Where

$$A = \begin{bmatrix} -\frac{R}{L} & -\frac{1}{L} & \frac{D}{L} \\ \frac{1}{C_2} & -\frac{1}{R_0 C_2} & 0 \\ -\frac{D}{C_1} & 0 & 0 \end{bmatrix} ; B = \begin{bmatrix} 0 \\ 0 \\ \frac{1}{C_1} \end{bmatrix} ; M = \begin{bmatrix} \frac{DV_{in}}{L} \\ 0 \\ -\frac{DI_L}{C_1} \end{bmatrix} \; ; \; C = [0 \quad 0 \quad 1] \; ; F = 0 \; and \; H = 0$$

(III.15)

The state-space averaged model that describes the nominal converter waveforms can be found using;

$$\begin{cases} 0 = AX + BU \\ Y = CX + FU \end{cases} \quad \text{(III.16)}$$

The steady-state solution of the converter is therefore

$$G_m = \frac{V_{in}}{I_{in}} = E(-A)^{-1}B + F \quad \text{(III.17)}$$

This equation yields: $G_m = \frac{R+R_0}{D^2}$

The recently equation represents the DC equivalent input impedance of the buck converter [4]. Referring back to the small signal model, the control to PV voltage transfer function can be obtained as

$$T_p = \frac{\hat{v}_{in}(s)}{\hat{d}(s)} = -\left(\frac{b_2 s^2 + b_1 s + b_0}{s^3 + a_2 s^2 + a_1 s + a_0}\right) \quad \text{(III.18)}$$

Where.

$$b_0 = \frac{DI_L}{L\,C_1 C_2} + \frac{(D^2 V_{in} + DI_L\,R)}{R_0\,L\,C_1\,C_2};\; b_1 = \frac{1}{C_1}\left(\frac{D^2 V_{in}}{L} + \frac{DI_L\,R}{L} + \frac{DI_L}{R_0\;C_1\,C_2}\right);\; b_2 = \frac{D\,I_L}{C_1};\; a_0 = \frac{D^2}{L\,R_0\;C_1\,C_2}$$

$$a_1 = \frac{R}{L\,R_0\;C_2} + \frac{1}{L\,C_2} + \frac{D^2}{L\,C_1} \cdot a_2 = \frac{1}{R_0\;C_2} + \frac{R}{L} \quad \text{(III.19)}$$

If we neglect the effect of the capacity C1,and R [10] the transfer function can be reduced to

$$T_p(s) = \frac{\hat{v}_{pv}(s)}{\hat{d}(s)} = \frac{\frac{I_L}{C_2}s + \frac{DV_{pv}}{L\,C_2}}{s^2 - \frac{1}{r_{pv}\;C_2}s + \frac{D^2}{L\,C_2}} = \frac{K(s+\tau)}{s^2 + 2\delta\omega_n s + \omega_n{}^2} \quad \text{(III.20)}$$

With

$$K = \frac{I_L}{C_2};\quad \omega_n = \frac{D}{\sqrt{L\,C_2}};\quad \delta = \frac{1}{2r_{pv}\,C_2\omega_n} \text{ and } \quad \tau = \frac{DV_{pv}}{L\,I_L}. \quad \text{(III.21)}$$

If we consider the following parameters of the converter DC-DC and PVG [11]:

$C_1 = 660\mu F$; $C_2 = 100\mu F$; $L = 120mH$ And $R_0 = 2.5\Omega$

Function region/Variables[12]	V_{pv}	**D**	I_L	r_{pv}

Region I	20	0.60	3.96	-0.2
Region II	16.5	0.73	6.66	-0.64
Region III	15	0.8	6.33	-1.95
Region IV	13	0.92	5.57	-9.83

The theoretical transfer function of PWM is simple as it can be seen ,while in practice, it always comes with some time delay [14]

$$T_m(s) = \frac{\hat{d}(s)}{\hat{v}_c(s)} = \frac{1}{\hat{V}_r} \tag{III.22}$$

$\hat{V}_r(s)$: Peak saw-teeth voltage in this work $\hat{V}_r = 1$

$\hat{v}_c(s)$: control voltage (which is always $0 < \hat{v}_c < \hat{V}_r$

$T_m\ (s)$: The transfer function of PWM modulator.

III.4.2 Open loop block diagram of the system

The open loop block diagram of the system, without compensator $T_1(s)$ can be seen in Fig. III.7

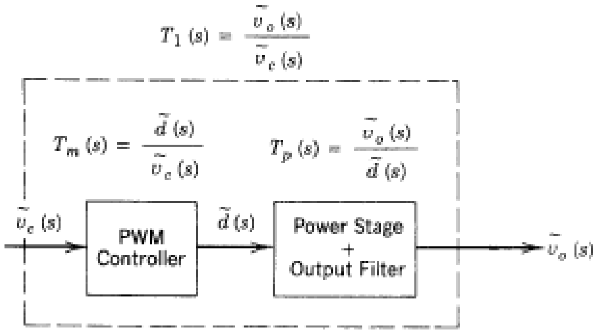

Fig. III.7 The open loop block diagram of the GPV-DC-DC converter with PWM.

III.5 Proposed System Design controller

Figure III.8 shows the overall system architecture. The proposed MPPT controller builds upon the simplicity of the P&O technique associated with PID regulation.

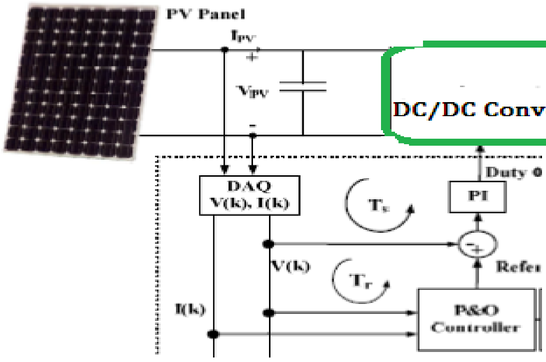

Fig. III.8 The proposed DSP based standalone solar energy system controller with PO code

III.5.1 PV Source with MPPT Code

Before implementing our control, we first simulate the PV model with the MPPT code given in Fig.III.9 .The Matlab MPPT code was discussed in section II.2. It is used to calculate the maximum amount of power that the PV source can output and maintain.

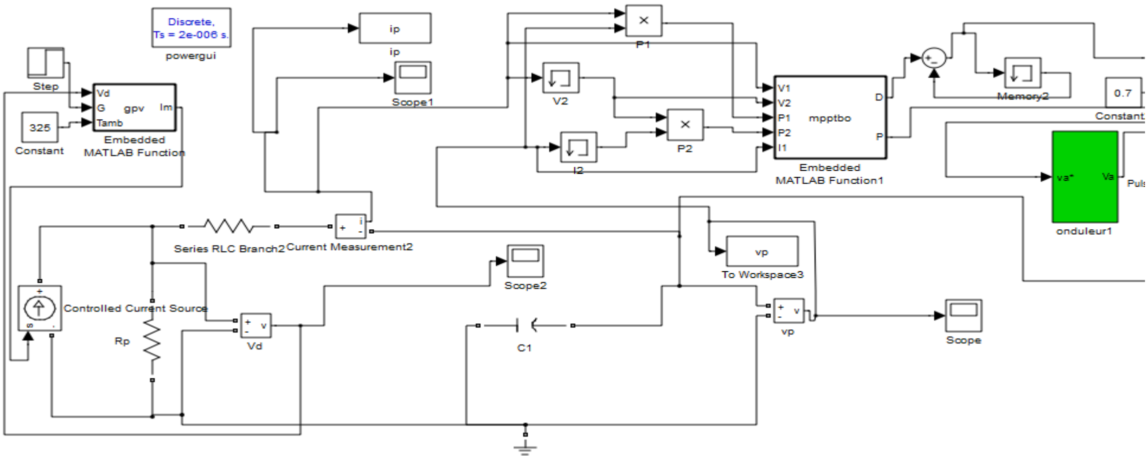

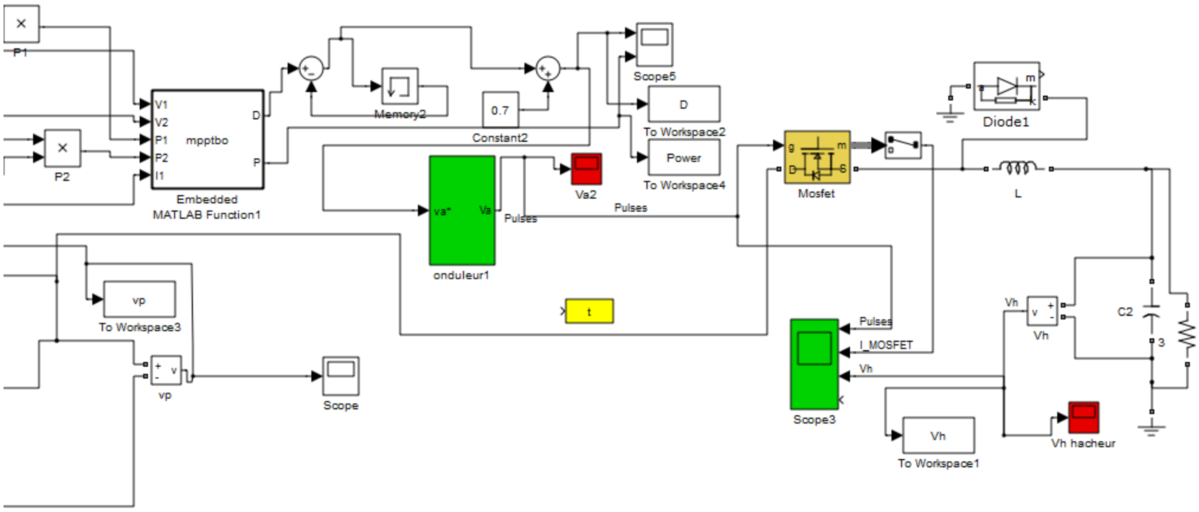

Fig. III.9 PV Source-DC converter with MPPT Code

Simulations results of the MPPT Code:

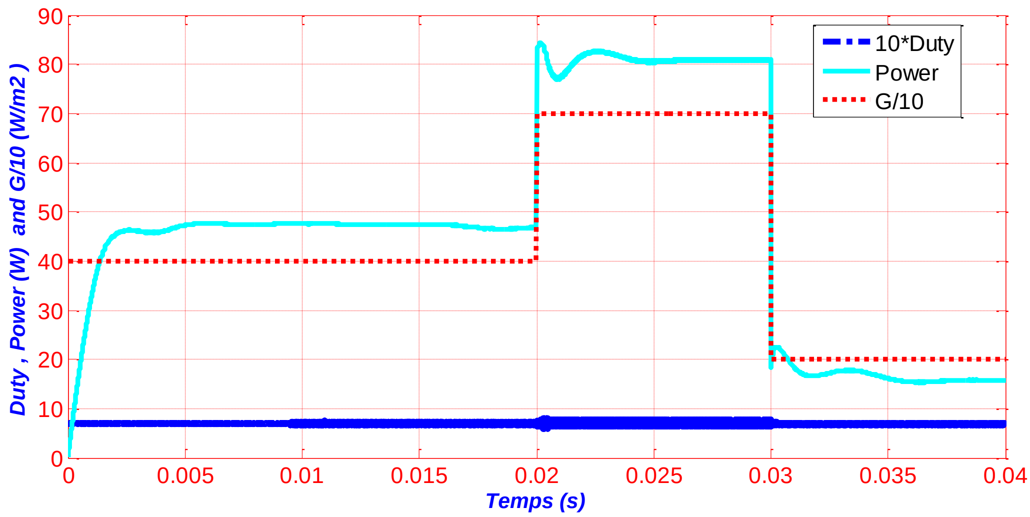

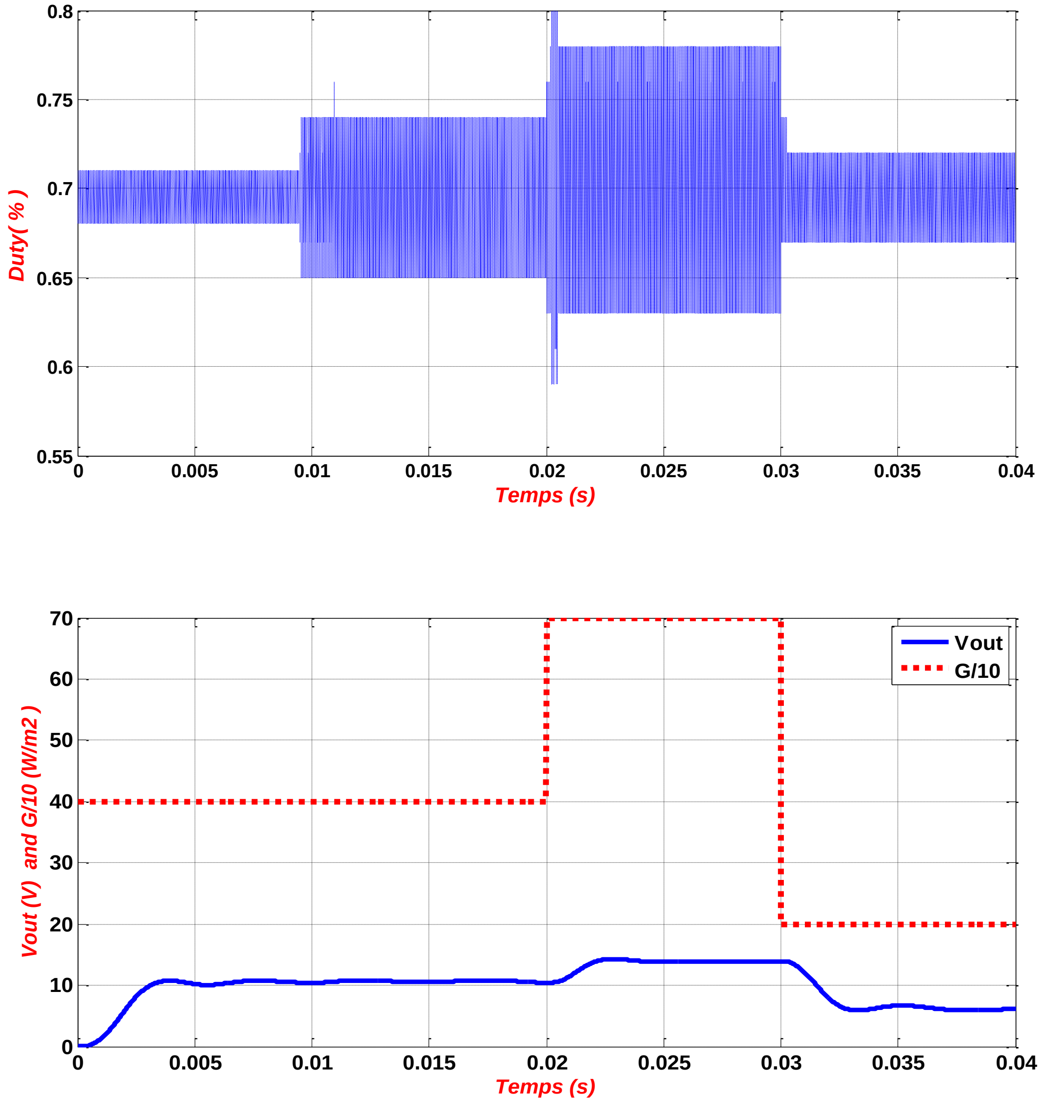

Fig. III.10 Responses of the GPV- DC-DC converter with MPPT Code

a) b) c)

III.5.2 Closed loop of the PV Source with MPPT Code

We start with some basic concepts:

The open loop function:

$$T_{OL}(s) = T_C(s)T_1(s) = T_C(s)T_p(s)T_m(s)$$

Closed loop transfer function $T_{CL}(s)$based on Fig III.8 would be

$$T_{CL}(s) = \frac{T_{OL}(s)}{1+T_{OL}(s)} \tag{III.23}$$

Where $T_C(s)$ is the amplifier transfer function.

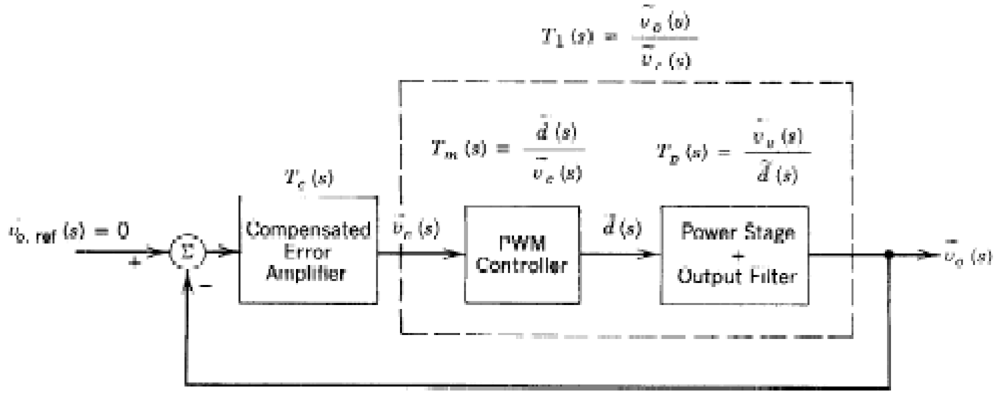

Fig. III.11 Closed loop block diagram

PID Regulator synthesis

$$T_c(s) = K_p(1 + T_d s)(1 + \frac{1}{T_i s})$$

$$= K_p/T_i s(1 + T_d s)(1 + T_i s) \qquad \text{(III.24)}$$

In order to assure the causality principle of the system, we take $(\frac{T_d s}{T_f s+1})$ instead of $T_d s$.

Observations and objectives desired:

First, by plugging the corresponding values to the transfer function obtained in the previous part, the open-loop transfer function can be obtained by (III.4):

We desire to have a system with following specifications objectives:

+ Phase margin higher than 60°

+ Gain margin higher than 20 dB

+ Over shoot less than 5%, (high overshoot is not suitable for batteries)

+ Steady state error less than 1%

+ Appropriate bandwidth or time response less than 3ms

Based on the quality of performances, we found the following parameters of the PID regulator:

$$T_i = 0.5 \cdot 10^{-3} \qquad T_d = \frac{1}{5.10^4} \qquad \Longrightarrow K_p \simeq 0.20 \qquad \text{(III.25)}$$

Simulations results

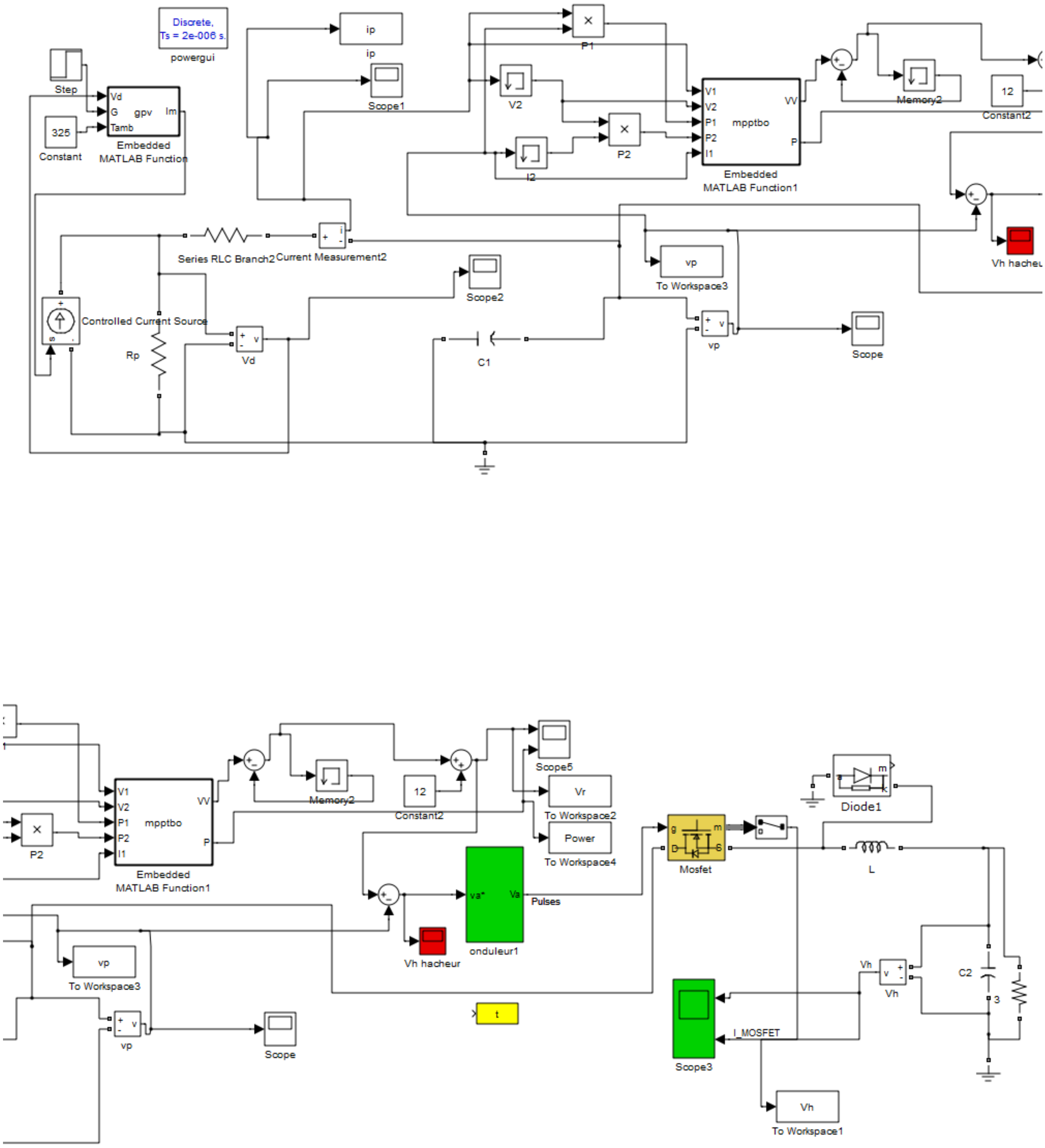

Fig. III.12 Constant voltage control of PV Source-DC converter with MPPT Code

Based on the choice of all parameters and Matlab/Simulink programs given in Fig. III.12, we obtain the simulation results responses, if we consider G=1000W/m^2, T=25% given in Fig III.13:

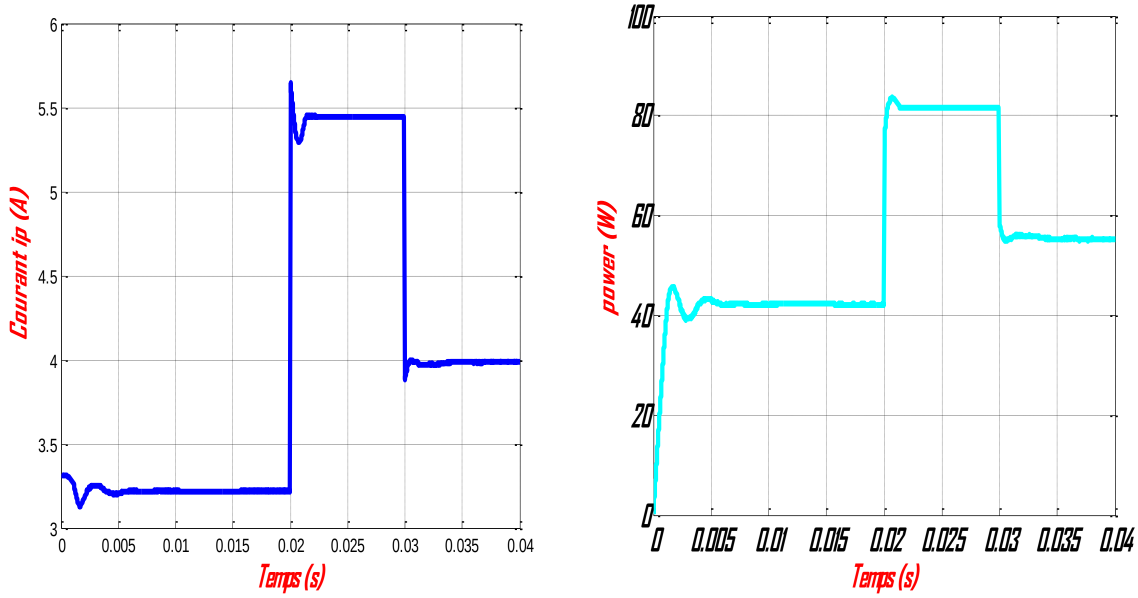

a)

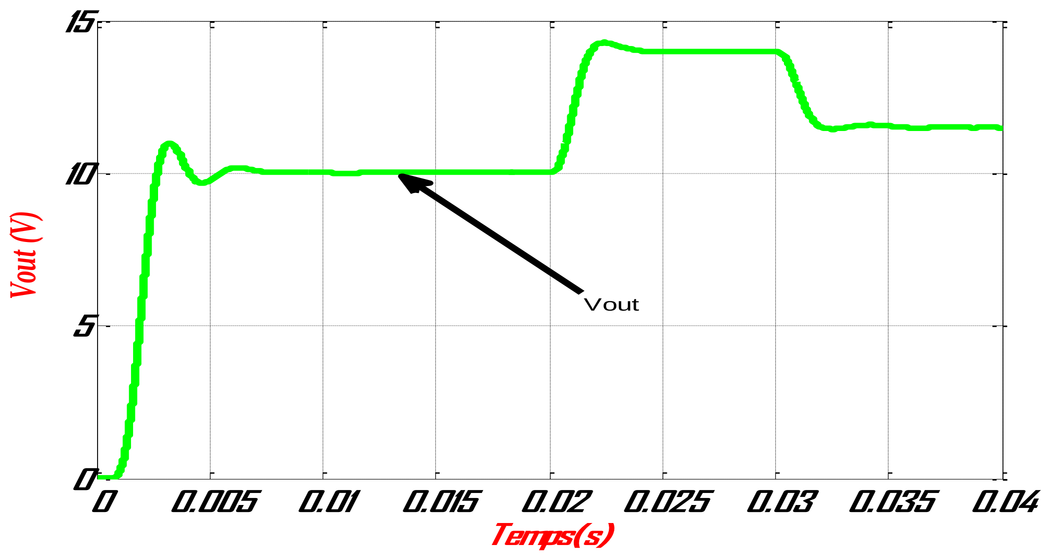

b)

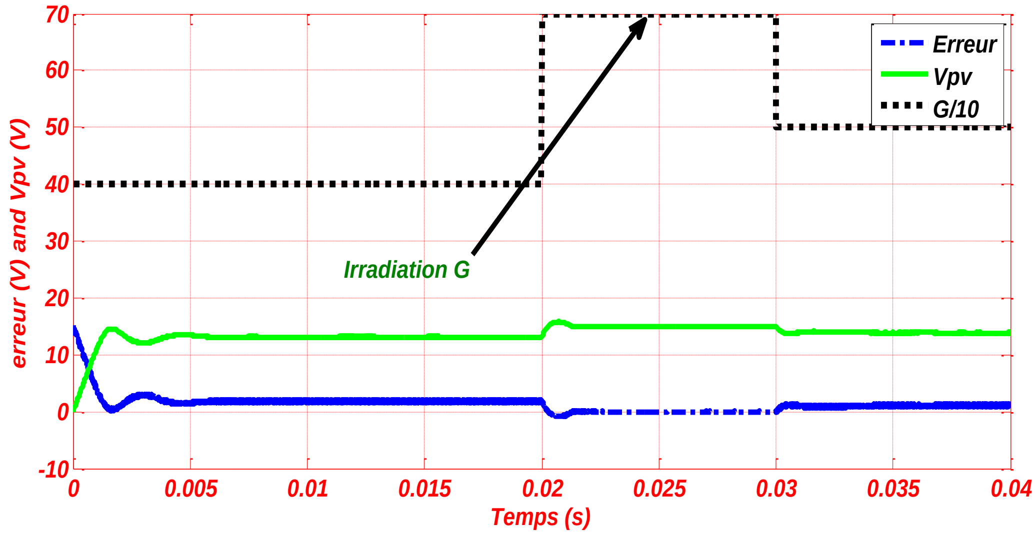

c)

Fig. III.13 Constant voltage control of PV Source-DC converter with MPPT Code

a) b) c)

.

It is therefore seen that no matter what the input voltage is from the PV source, our design accurately and successfully can calculate the maximum power and maintain this as a constant, until the input voltage changes again and the process is repeated.

III.6 Summary

This chapter provides the design and MATLAB simulation of the proposed PV-DC-DC converter system to test the performance of the proposed MPPT techniques and to verify their functionality. The system comprises of PV array, DC-DC buck converter, MPPT controller and resistive load. Each of these components has simulated and masked in an individual subsystem so can be easily controlled and precisely monitored. Then, these subsystems are combined to form the complete system.

First, to verify the functionality of the proposed VC-P&O MPPT algorithm and compare its performance against the conventional P&O algorithm, they were implemented in MATLAB with a resistive load. The simulation was performed under rapidly varying solar irradiation levels starting at 400 W/m2 to be increased to 700 W/m2, and then decreased to 500 W/m2 again. The results show that the CV-P&O has significant improvement compared with the P&O. The results proved that the CV-P&O has improved the tracking speed and has increased the oscillation around the MPP in steady state.

Chapter IV:

Design and implementation of the P and O around Atmel microcontroller

IV. 1. Design Introduction

Once the DC/DC converter component values were decided and the MPPT method chosen, the next step was to simulate our design for the overall project. This was done in stages based on the main sections in the following .The entire project would consist of a PV source that acts as the input for the DC/DC buck converter. This is the input for the microcontroller, which receives the voltage and current values and calculates the maximum power based on that information. Once that is gathered, the duty cycle of the DC/DC converter must be adjusted to maintain that maximum voltage. The microcontroller adjusts the converter duty cycle by the PWM, which is another input for the converter. The following sections explain the code used to calculate and maintain the power, and how it was designed and implemented in Matlab Simulink.

IV. 2. Matlab Code

One of the key factors of this project was the MPPT algorithm and the way this algorithm implemented on our system. As it was mentioned before, perturb and observe method was chosen to perform the tracking of maximum power point. This method was based on the electrical power that was calculated with voltage and current from DC/DC converter and then, it compared the power at each moment and tracked the maximum power by modifying the duty cycle of the system. To implement this algorithm, Matlab software was used to simulate the whole system and test out the code before implementing it practically. Matlab software was chosen due to its ability to simulate and code in one file. Using the flowchart of the algorithm, the code was written step by step [5].

The instantaneous power delivered by the solar panel at each moment was calculated by measuring the output voltage and current across the DC/DC converter and multiplying both quantities. This function executed in a loop so that it would be repeated and produced multiple power readings. Modifying the duty cycle would change the operating voltage and the power would be calculated again, which would always result in maximum power point.

IV.3 Buck Converter Design:

The design was done for a 85W solar panel and 12V battery was taken as the output. While designing a buck converter important factors are switching frequency and filter design. Higher the switching frequency means smaller will be filter size which thereby means smaller will be inductor and capacitor size which reduces the overall cost. But the problem is that if switching frequency is too high that will increase switching losses in the MOSFETs and thus reduces the efficiency so it is important that compromise has to be done between these factors. Here PWM frequency taken was 30 kHz. Buck converter comprises :1. Inductor 2. Capacitor 3. MOSFETS. Based on :

-Technical characteristics of the PV solar panel

Number of cells	**36 in series**
Open circuit voltage ($\boldsymbol{V_{OC}}$)	21.6V
Short circuit current ($\boldsymbol{I_{CS}}$)	5.16A
Voltage of MPP($\boldsymbol{V_{mpp}}$)	16.75V
Current of MPP ($\boldsymbol{I_{mpp}}$)	4.78A
Maximum power ($\boldsymbol{P_{mpp}}$)	80W

-Performance design for an 85W solar panel and 12V battery as output and

Inductance L $\Delta i_L = 400mA$

Condenser terminals $\boldsymbol{C_2}$ $\Delta V_{C2} = 10mV$

Condenser terminals $\boldsymbol{C_1}$ $\Delta V_{C1} = 100mV$

$f = 100kHz$

We can evaluate the Initial Duty cycle :

$$D = \frac{V_{load}}{V_{PV}} = \frac{12}{16.75} = 0.716 \qquad \text{(IV.1)}$$

Equivalent resistance Load R_{eq}:

$$R_{eq} = \frac{{V_{load}}^2}{P} = \frac{12^2}{80} = 1.8\Omega \qquad \text{(IV.2)}$$

IV.3.1 Calculations for the buck filter :

-Inductor Design

Inductor is used to reduce the ripples in current, thus smooth waveform of current can be obtained. So it is very important that the value of inductance chosen is such that it can efficiently satisfy our requirements.

Assumption: We are designing for a 85W solar panel and 12V battery

Input voltage $(V_{in}) = 17V$

Output Voltage$(V_{out}) = 12V$

Output current$(I_{out}) = 85W/12V$=7.1A

Switching Frequency $(f_S) = 30Khz$

Duty Cycle $(D) \ = Vout/Vin = \ 12/17 \ = 0.7 \ or \ 70\%$

Calculation

$$L = \ (V_{in} - V_{out}) \ \cdot \ D \ \cdot \ 1/fs \ \cdot \ 1/\ \Delta I \qquad \text{(IV.3)}$$

Where ΔI is Ripple current

Typical value of ripple current is in between 10 to 15 % of load current.

Let $\Delta I \ = 10\%$ of rated current

$\Delta I \ = 10\% \ of \ 7.1 = 0.1 \ x \ 7.1 \ = 0.71A$

So $L = \ (17.0 - 12.0) \ \cdot \ 0.7 \ \cdot \ (1/30Khz) \ \cdot \ (1/0.833) \ = \ 160.55uH$

$Inductor\ peak\ current \ = Iout \ + \ dI/2 \ = \ 7.1 + \ (0.71/2) \ = \ 7.75A$

A toroid inductor of 160.55uH and 5A was made.

As the inductor we are using is made with a circular metal ring and coil, the number of turns the coil needs is necessary to get the correct 160 uH needed. The equation below finds the number of turns needed

$$L = \frac{r^2 turn^2}{9r + 10l} \qquad \text{(IV.4)}$$

Where r is radius of the hole of the metal ring, l is length/thickness of the ring, and L is inductor value. Rearranging this, the number of turns can be found:

$$turn = \sqrt{\frac{L(9r + 10l)}{r^2}} \qquad \text{(IV.5)}$$

Using r=1.5cm, l=1cm, and 160 uH, the number of turns is found to be 64 turns. This means our inductor has 64 windings on the metal ring.

IV.3.2 Output and Input Capacitors Design C1 and C2:

Capacitances were used to reduce both the overshoots in voltage and ripples in the output and input of buck converter. So it is mandatory that even the values of capacitance should be such that it can sufficiently meet our system's requirements.

Calculation of C1 and C2:

The output capacitor $C_2 = \Delta I \,/\, (8 \cdot fs \cdot \Delta V)$ (5)

Where dV is ripple voltage

Let voltage ripple $\Delta V = 30mV$

$C_2 = 0.47/\,(8 \cdot 30000 \cdot 0.03) = 210.75\, uF$

And C_1

$$C_1 \geq \frac{I_{PV}}{\Delta V_{PV.max}.\, f} \Rightarrow C_1 \geq \frac{4.78}{10^{-1} \cdot 10^{4}} \Rightarrow C_1 \geq 478\mu F \tag{IV.6}$$

IV.4 Data acquisition by a voltage divider:

When trying to read the output voltage of the buck converter, there was a problem that we encountered. The Arduino **Uno or Mega 2560** was the chosen component to perform the power calculation and the MPPT algorithm. The analog pins of the Arduino can only read the voltage from a range of 0-5V. However, the requirement for the prototype is to be able to read the voltage with a range of 0-25V. Therefore, to solve this problem, we decided to use voltage divider to change the voltage going into the input pin of the Arduino to no larger than 5V. The reduced voltage will get converted back to its original value based on the voltage divider ratio before the Arduino uses that value to compute the power

IV.4.1 Voltage Measurement:

For a voltage divider circuit

$V_{out} = R2/\,(R1 + R2) \cdot V_{in}$

$V_{in} = (R1 + R2)/R2 \cdot V_{out}$

The analog Read ( ) function reads the voltage and converts it to a number between 0 and 1023

The above code gives an ADC value in between 0 to 1023

Calibration:

Output value is read with one of the analog inputs of Arduino and its analog Read() function.

That function outputs a value between 0 (0V in input) and 1023 (5V in input) that is 0,0049 V for each increment (As 5/1024 = 0.0049 V)

$V_{in} = (R1 + R2)/R2 \cdot V_{out}; R1 = 100\ k\Omega\ and\ R2 = 20\ k\Omega$

$V_{in} = ADC \cdot 0.0049 \cdot (120/20)$ Volt .

The voltage measurement can be achieved using LV 25-P voltage transducer with an input/output current of 10mA/25mA. The resistance Rp of the voltage transducer in Fig (IV.1) was calculated according to the maximum measured voltage

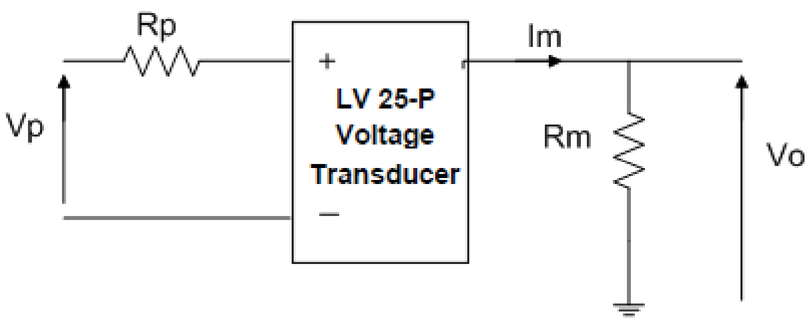

Fig. IV.1 Voltage Transducer Signal Conditioning Circuit

IV.4.2 Current Measurement

Current measurement is employed based on Hall-effect transducers. The current measurement was achieved using LA 100-P Hall-effect current transducer with a ratio of 100A/50mA, shown in Fig (IV.2). The transducer ensures complete isolation between the power and control circuit. The resistance value (Rm) in both transducers was chosen to ensure that the output voltage from the transducers does not exceed 3.3V (the maximum analogue input range of the DSP. For low current measurements, the resolution of the transducer is further increased by decreasing the number of primary side turns to achieve a suitable output voltage at low current values. The sensor can measure positive and negative currents (range -5A…5A), 3. Power supply is 5V 4. Middle sensing voltage is 2.5 V when no current. Calibration: Value = (5/1024)*analog read value Current in amp = (value-2.5)/0.185.

The voltage measurement can be achieved using LV 25-P voltage transducer with an input/output current of 10mA/25mA. The resistance RP of the voltage transducer in Fig (IV.2) was calculated according to the maximum measured voltage.

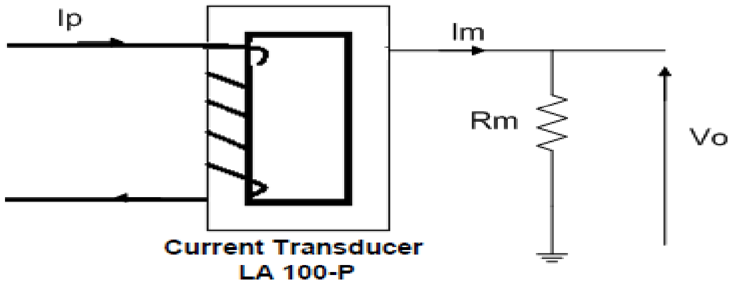

Fig. IV.2 Current Transducer Signal Conditioning Circuit

IV.4.3 Amplifier and Driver choice

Amplifier

It is necessary to choose an amplifier to satisfy speed and requirement for voltage and currents to adjust and adapt all values to 5Volts.Our choice was an LM 358 given bellow.

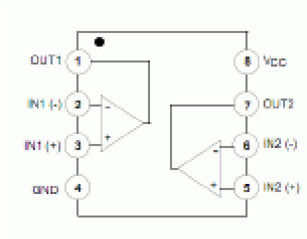

Fig. IV.3: LM 358 amplifier used in MPPT tracking.

Driver

To isolate the DSP ground from the power circuit ground, an optocoupler 6N137 was used to achieve isolation between the gate signals from the DSP to the power switch of the power circuit. The circuit configuration is shown in Fig (IV.4).

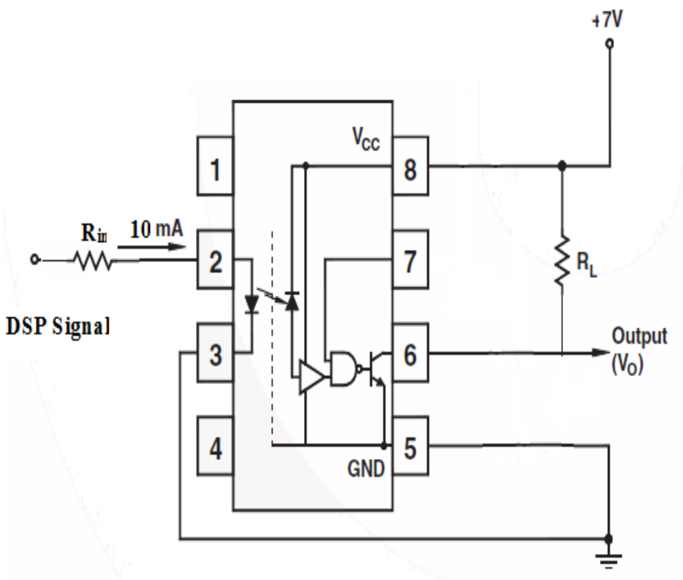

Fig. IV.4 The Circuit Configuration of the optocoupler (6N137)

Where Rin = 330Ω to limit the input current to 10 mA, RL = 1kΩ to protect the (VCC) supply from short circuit condition.

IV.5 Implementation/ Monitoring Performance

For our project, an Arduino needed to perform three distinct functions and those were as follows:

1. Provide the correct frequency of the PWM square wave,
2. Calculate the power using the current and voltage reading obtained from the DC/DC buck converter every time,
3. Implement 'Perturb and observe' algorithm that compared the previous power to new power and modified the duty cycle of PWM to track the maximum power point successfully.

Setting up the PWM of the Arduino can get complicated because each PWM pin was set with a default frequency that was much lower than our operating frequency. Pin 9, for example, had a default frequency of 490.2 Hz, while our system required an operating frequency of 30 kHz. To increase the operating frequency of the specific PWM pin, another line of code had to be written. Depending on which pin was used, the timer varied and depended on the timer divisor, the frequency varied as well. According to the Arduino page, pin 9 uses timer 2.

As the operating frequency of the project was 30 kHz, so the closest possible frequency to 30 kHz was 31372.55Hz for the Arduino pin 9. According to the table, 31 kHz is controlled by the timer 1 divisor. To set the timer 2 divisor to 1 for PWM frequency of 31372.55Hz ≈ 31.4 kHz, a code was written in the setup function:

TCCR2B = TCCR2B & B11111000 | B00000001;

This code changed the frequency of pin 9 to 31.4 kHz. The duty cycle in the Arduino is defined on a scale of 0 – 255 where 0 is always off and 255 is always on 100%. The source voltage of 17V stepped down to 12V by the buck converter, which gave us a duty cycle of 70% and this corresponds to 178 in Arduino. To assign our PWM Pin duty cycle to 70%, another line of code was written in the loop function:

analog Write (PWM Pin, 178);

This allowed the initial square wave to be at 70% duty cycle. To make sure that PWM Pin successfully provided 70% duty cycle signal with 31kHz, the oscilloscope was connected and the frequency and pulse were monitored.

For our project, the duty cycle of the signal needed to be modified depends on the voltage input to track the maximum power point successfully rather than staying at 70% duty cycle the whole time. Hence, the code needed to be modified as follows:

Analog Write (PWM Pin, duty cycle);

The variable duty cycle was declared and initially assigned to 178 and it would increase or decrease depends on the power value. Another variable change D was assigned and it represents the amount of change of the duty cycle. For this project, the step size was set to be 5%, which is corresponding to 12.7 in Arduino code. For example, if the duty cycle needed to increase, it would increase by 5% from whatever value duty cycle was at and vice versa.

After successfully implementing the function for setting up the PWM signal for the switch of the buck converter, Arduino needed to calculate the power output by using the voltage and current from the buck converter. To read the voltage output from the buck converter, the analog input pin, A1 was assigned to the voltage output port on DC/DC converter. As the voltage reading from Arduino would be in a raw data value (0 - 1023), it should be converted into a voltage reading (0 - 5V). This could be done by the following code [7]:

$voltage\ =\ ((float)raw\_voltage\_data\ \cdot\ 5.0)\ /\ 1023.0$

As the Arduino Mega 2560 can read the voltage up to 5.0V only, the voltage divider has been added. Hence, the voltage read from the analog input should be multiplied by the voltage ratio. A current was calculated by dividing the voltage by the load resistor, 1.5 ohms as the current in the resistor is equal to the output current according to the Kirchoff's Current Law. These voltages and current values then entered through the Arduino to compute power.

To compute the power, a few variables were declared: P for power, V for voltage and I for current and using these variables, the power formula was written:

$P\ =\ V\ \cdot\ I;$

After it executed the formula and calculated the power output, the P&O algorithm was implemented. The code for the algorithm was written based on the flowchart of the algorithm and the Matlab code that was written for the simulation.

The implementation of P&O algorithm was the major function of the Arduino. This algorithm processed by changing the duty cycle of the PWM that controls the MOSFET from 0% to 95% in increments of 5%. The change in the PWM would affect the output voltage of the DC/DC converter and alter the power output. As the voltage and current changes, the power calculations are made and recorded with each increment until it reaches maximum power. Once it reaches the maximum power point, it maintains the duty cycle value where the maximum point is recorded and maintains the maximum power point. If there is any change in the voltage or current value, change the power output to be bigger than the previous maximum power point that was found, the algorithm will be executed again and change the previous maximum power point into the new power output and vice versa.

IV.6 THE PROPOSED SETUP

IV.6.1 Overall System and schematic circuit

The configuration shown in Fig IV.5 shows the architecture of the experimental test rig consisting of the following elements:

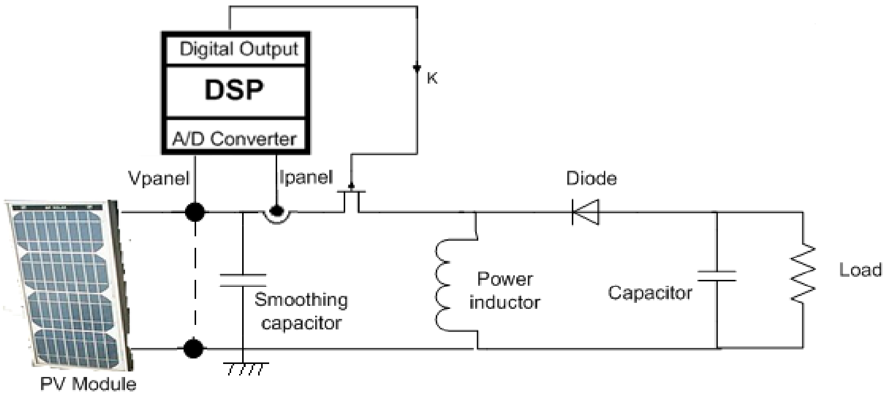

Fig. IV.5: The Overall System Hardware Implementation

a- PV Module

Since the study is intended for renewable energy applications, a photovoltaic module (Model: ASE -300-DGF/17) with the specifications and characteristics is used for testing the control technique and operation algorithm.

At nominal ratings (1000w/m2 irradiance, temperature 25^{o}c), the open circuit voltage (VOC) is equal to (20V), the short circuit current (ISC) is equal to (18.4 A), the voltage at the MPP (VMPP) is equal to (17 V), the current at the MPP (IMPP) is equal to (16.8 A) and the maximum power (PMPP) is equal to (285 W).

b- Arduino

Table (5.1) Main specifications of Arduino controller

Clock frequency	16MHz
Available PWM Channels	2x 9 channels
ADC channels	12bit 8x 2 channels
ADC Conversion time	80ns
RAM	68kB

Experimental Setup and schematic electronic circuit

The system photograph shown in Fig IV.6 and schematic electronic circuit Fig IV.7 and Fig IV.8 illustrate the connection of the implemented system with the all connected elements.

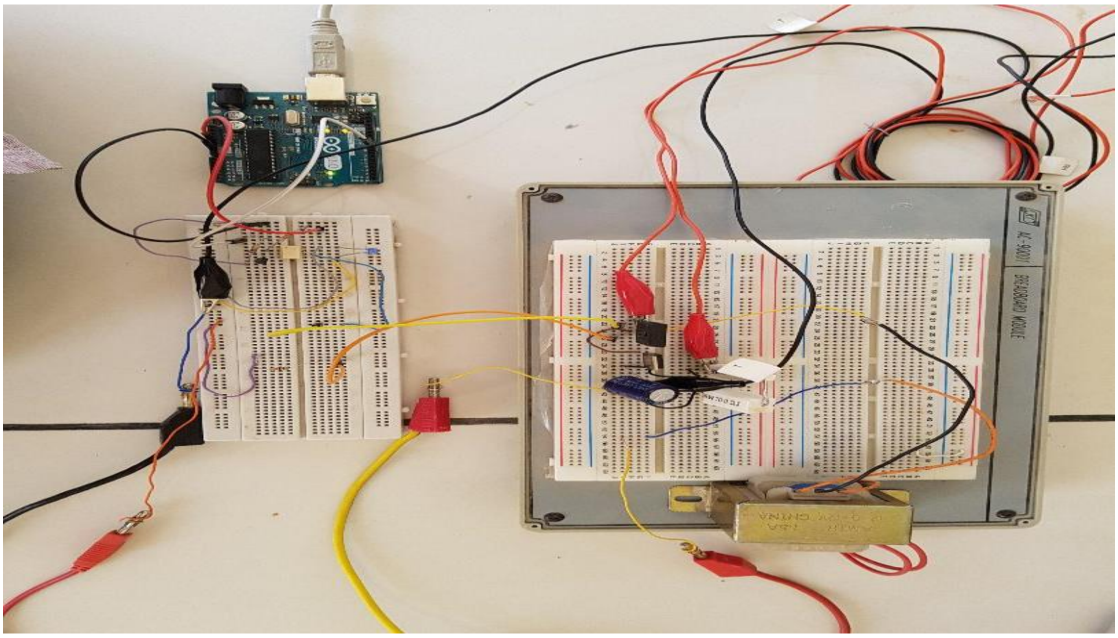

Fig IV.6 Arduino and Experimenter Board

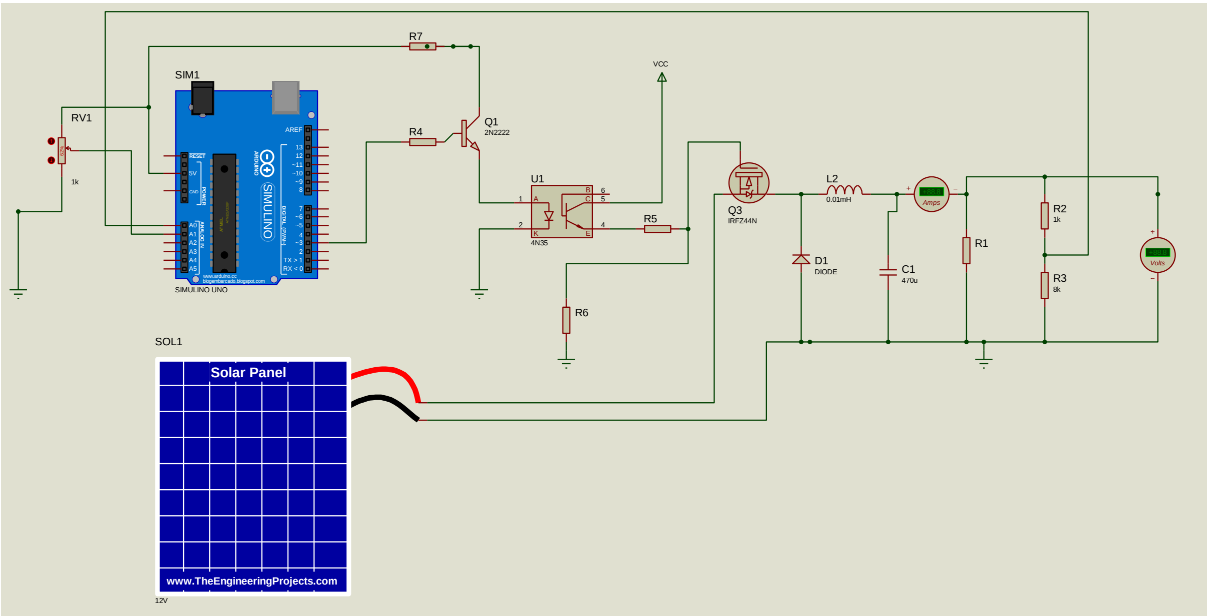

Fig. IV.7 Circuit diagram of charger circuit

The system consists of the following components:

A. Laptop Programmer.
B. Arduino Mega.
C. Isolation Circuit.
D. Power supply for transducer circuit.
E. Power transistor MOSFET.
F. Honeywell LA 50A current transducer circuit.
G. voltage divider transducer circuit.
H. Power inductor.
I. High Frequency Reverse diode.
J. Power Switch.
K. Variable Resistive load.
L. Oscilloscope.
M. PV Panel.

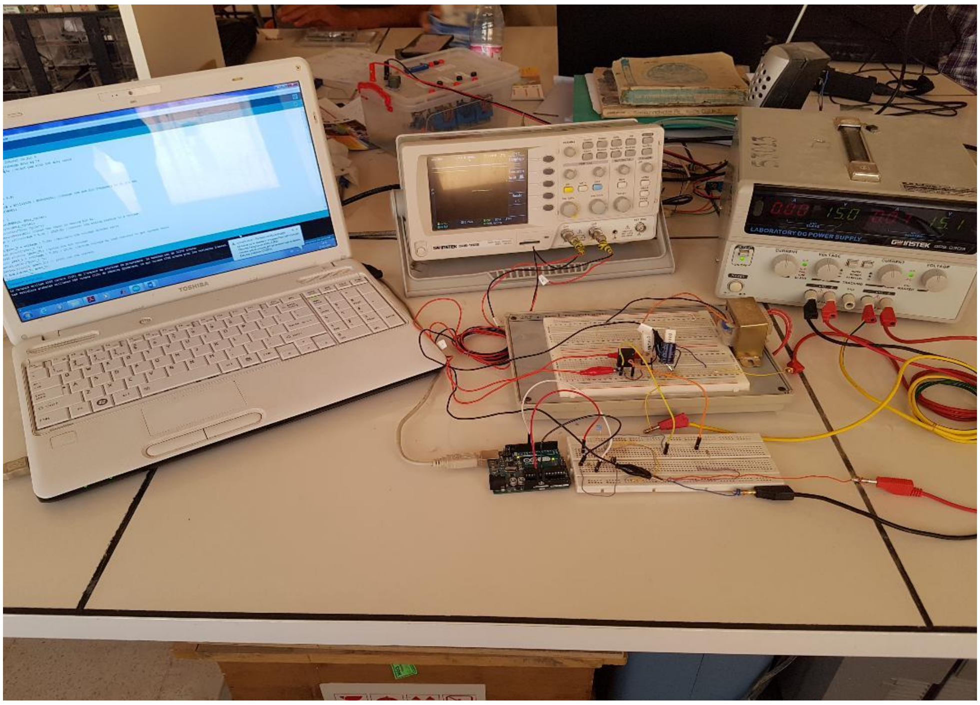

Fig. IV.8 Photograph of the Implemented System

VI.7 RESULTS AND DISCUSSION:

The 5V supply is given to microcontroller ATMEGA 328 by the laptop. The output of the microcontroller provides gate pulse to MOSFETs but this voltage is not sufficient to provide triggering of the MOSFET so MOSFET driver is required here.

The frequency generated is f=31 KHz. This is the gate pulse given to the MOSFETs.

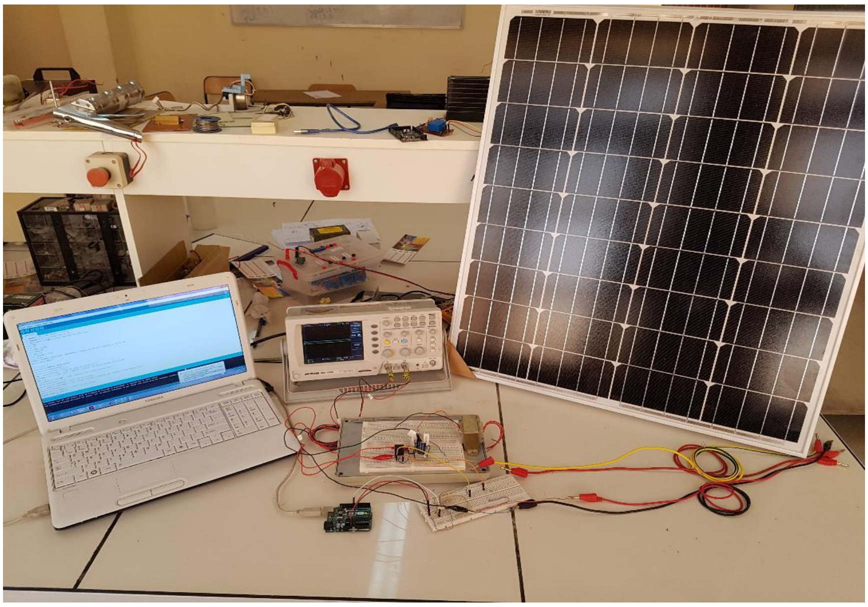

Fig. IV.9 Testing of the Buck Converter (Output Voltage)

As shown above Fig. IV.9, it successfully stepped down the 17V to roughly 11.4V, which is very close to the expected value of 12V. The ripple of the voltage output was very small, about 500mV.

To test the final product, all the components were connected together and the Arduino was connected to the laptop with a USB. The code was uploaded to the Arduino through the IDE and the data of the output power was displayed on the laptop screen through the serial monitor feature of the IDE.

IV.8 Conclusions and Improvement

Over hours of research, applying theory and practice, and after many failures, the prototype finally functions with 40%. The prototype successfully locates the maximum power regardless of what the solar panel voltage production may be which can be improved. Hence, this prototype can be used to track the maximum power point of different solar panels and help customers determine the most efficient solar panels available Although the final project does not function as expected, there's still some improvements. There are few chosen components that were used for the prototype that could be chosen differently for better performance. For example, the load resistor can have the same resistance value but should be able to withstand higher power output. Currently the resistors' temperature can be very high if the maximum power is too high. Another adjustment could be to try out different types of capacitors, with and without parasitic, to see which type of capacitor would be better. We had hoped to do this but unfortunately ran out of time. Another improvement would be to use a different microcontroller as STM32F407. The Arduino Uno and Mega 2560 uses a language that is very simple to program and there are many available resources, however, the actual chosen hardware was not very compatible with our circuit. Therefore, choosing a different microcontroller that better fits the circuit would help improve the accuracy of measuring and calculations as well as simplifying the overall circuit and the code, as mentioned in design modification section. We can ,also use an interface should be a LCD screen that can display all the desired values and the user-desired plot. These are all possible improvement points that can be accomplished if there had been more time, or these can be done in the future.

CONCLUSIONS AND FUTURE WORKS

Conclusions

In this research, a stand-alone photovoltaic system is presented to supply areas with a clean and sustainable source of energy. The main focuses of this research was how to improve the total system efficiency by implementing an efficient MPPT techniques to transfer the maximum available power to the load especially under rapidly changing atmospheric conditions.

The thesis reviewed and discussed some existing MPPT controller methods, including constant voltage and P&O method and showed their ability to track the MPP under rapidly changing weather conditions. It illustrated the advantages and disadvantages of each individual MPPT technique tracking performance.

The MPPT controllers proposed were analyzed and developed in more depth using new system simulations to clearly show improvements. The proposed technique is a perturb and observe P&O technique. The P&O MPPT method is very simple in comparison with other techniques, which makes it the easiest to design and implement. The CV method was shown to have a faster dynamic response and eliminates the steady state with oscillation around the MPP thereby; it improves the MPPT efficiency of the PV system. The design and results of the developed P&O and CV MPPT technique were presented and explained.

The simulation results were presented in order to show the benefits of MPPT and evaluate the performance and functionality of the proposed MPPT techniques. The simulations were performed using MATLAB/SIMULINK. A model of the complete PV systems was presented and discussed along with how all of the masked components have been combined to form this system. A more detailed SIMULINK model of each component was also presented, starting with the PV solar panels, buck converter, DC load and MPPT controllers, and then each component masked within a subsystem.

The simulation results were divided into two parts: in the first part the PV system is feeding a resistive load to evaluate and test the performance of the modified P&O and CV algorithm. The simulation results clearly showed that, the P&O has the ability to improve both the steady-state and dynamic performance of photovoltaic power generator systems. Performance was assessed with rapidly changing solar irradiation conditions.

Contributions

The major contributions of this thesis are:

The proposed perturb and observe (P&O) MPPT method with CV method. The conventional P&O was modified to overcome the drawbacks in the conventional P&O MPPT algorithm. This is done by combining the conventional P&O with CV-Control. A comparison with conventional P&O MPPT algorithm showed that the proposed algorithm has improved both the steady-state and dynamic performance of the photovoltaic power generator systems.

Future works

1-Other control technics as, Neuro-Fuzzy ,sliding mode and other MPPT controller could be an alternative or a solution to improve the performance.

2-Implementation of the PV water pumping system and connection to the grid should be treated.

3- Future research could investigate some other converters such as boost, buck and buck-boost along with the proposed MPPT techniques to improve flexibility in the choice and configuration of PV array connection.

In this work, simulation models were developed and used to compare the performance of the proposed MPPT techniques. However, practical hardware tests at a representative power level and under the typical climatic conditions of an application have been conducted to verify the simulation results. The simulation results achieved in this work will hopefully urging future investigations involving building other prototype models to test experimentally the developed MPPT techniques for the PV system around more sophisticated microcontrollers such as STM32F429.

Appendices

MPPT Code Implemented in the Arduino

```
int PWMPin = 9; //PWM Connect to pin 9
int changeD = 12.7; //change duty by 5%
int duty_cycle = 127.0; //start pwm with 50% duty cycle
float Vm;
float P;
float prev_P = 0;
float prev_V;
int sum = 0;
float voltage = 0.0;
void setup() {
TCCR2B = TCCR2B & B11111000 | B00000001; //change the pwm pin frequency to 31.372
kHz
Serial.begin(9600);
}
void loop() {
analogWrite(PWMPin, duty_cycle);
Serial.print(duty_cycle);
Serial.println("Duty Cycle");
sum = analogRead(A1); //read the input on analog pin A1
voltage = ((float)sum * 5.0) / 1023.0; //convert the analog reading to a voltage
sum = 0;
float prev_V = voltage * 7.33; //multiply the voltage divider ratio
Serial.print("prev_V ");
Serial.println (prev_V); //print out the voltage
float prev_I = (voltage * 7.33) / 10.5; //divide voltage by load resistor to get current value
Serial.print("prev_I ");
Serial.println (prev_I); // print out the current
P_and_O(prev_V, prev_I);
Serial.print(P);
Serial.println("Watt");
Serial.println(" ");
```

```
delay(1000);
}
float P_and_O(float V, float I) {
P = V * I;
float changeP = P - prev_P;
float changeV = V - prev_V;
if (changeP != 0) {
if (changeP > 0) {
if (changeV > 0) {
if (0 <= duty_cycle && duty_cycle < 241.3) {
duty_cycle = duty_cycle + changeD;
}
else {
duty_cycle = 254;
}
}
else {
if (0 <= duty_cycle && duty_cycle < 255) {
duty_cycle = duty_cycle - changeD;
}
else {
duty_cycle = 241.3;
}
}
}
```

62

```
else {
if (changeV > 0) {
if (0 <= duty_cycle && duty_cycle < 255) {
duty_cycle = duty_cycle - changeD;
}
else {
duty_cycle = 241.3;
}
}
else {
if (0 <= duty_cycle && duty_cycle < 241.3) {
```

```
duty_cycle = duty_cycle + changeD;
}
else {
duty_cycle = 254;
}
}
}
}
else {
duty_cycle = duty_cycle;
}
prev_V = V;
prev_P = P;
return P;
}
```

REFERENCES

[1]**Antonio Luque and Steven Hegedus,"**Handbook of Photovoltaic Science and Engineering", John Wiley & Sons Ltd, 2003

[2] **Falk Antony, Christian Düshner Et Karlheinz Remmers,** " Le photovoltaïque pour tous Conception et réalisation d"installation ", livre édité par : INES), 2006.

[3] **F. Kininger,** "Photovoltaic Systems Technology", University of Kassel, 2003.

[4] **Anne Labouret, Michel Villoz**, "Energie Solaire Photovoltaïque (2 _eme édition)", Dunod, 2003.

[5] **R.A. Messenger, J. Ventre,** "Photovoltaic Systems Engineering (Second Edition)", CRC Press,2004

[6] **T.DenHerder,** "Design and Simulation of Photovoltaic Super System Using Simulink", California Polytechnic State University, 2006.

[7] **Hannes Knopf**, "Analysis, Simulation and Evaluation of Maximum Power Point Tracking (MPPT) Methods for a Solar Powered Vehicule", Portland State University, 1999

[8] **Harish, A., Prasad, M.V.D**. "Microcontroller Based Photovoltaic MPPT Charge Controller" (April 2013). Retrieved from International Journal of Engineering Trends and Technology

[9] **Hart, D. W.** (2011). "Power Electronics" P. 196-256. New York: McGraw-Hill.

[8] **T. Tafticht, K. Agbossou, M. L. Doumbia, and A. Cheriti,** "An improved maximum power point tracking method for photovoltaic systems," *Renewable Energy*, vol. 33, no.7, pp. 1508-1516, 2008

[9] **D. Jaume et M.Vergé**, "Le calculateur numérique pour la commande des processus", Techniques de l'ingénieur.

[10] **J. Martinez Garcia-Tenorio**, "Digital Control Techniques for DC/DC Power Converters", Helsinki University of Technology, 2009

[11] **Eftichios Koutroulis, Kostas Kalaitzakis, Member, IEEE, and Nicholas C. Voulgaris**, "Development of a Microcontroller-Based, Photovoltaic Maximum Power Point Tracking Control System", IEEE TRANSACTIONS ON POWER ELECTRONICS, VOL. 16, NO. 1, JANUARY 2001

[12] **K.J.Äström,** "From Control System Design : PID Control ", 2002

[13] **A.Visioli,** "Practical PID Control ", Springer, 2006